REVISED: CURRENT PHARMACEUTICAL DESIGN
Special issue on: ”Mitochondrial Biogenesis: Pharmacological approaches”

REGULATION AND QUANTIFICATION OF CELLULAR MITOCHONDRIAL MORPHOLOGY AND CONTENT

Karl J. Tronstad[1,#], Marco Nooteboom[2,#], Linn I. H. Nilsson[1], Julie Nikolaisen[1], Maciek Sokolewicz[2], Sander Grefte[2], Ina K.N. Pettersen[1], Sissel Dyrstad[1], Fredrik Hoel[1], Peter H.G.M. Willems[2] and Werner J.H. Koopman[2,$]

[1]Department of Biomedicine, University of Bergen, Bergen, Norway.
[2]Department of Biochemistry (286), Nijmegen Centre for Molecular Life Sciences, Radboud University Medical Centre, Nijmegen, The Netherlands.

[#]**Author contributions:** These authors share the first authorship.

[$]**Correspondence:** Dr. W.J.H. Koopman, 286 Biochemistry, Nijmegen Centre for Molecular Life Sciences, Radboud University Medical Centre, P.O. Box 9101, NL-6500 HB Nijmegen, The Netherlands, Tel: +31-24-3614589, Fax: +31-24-3616413, E-mail: w.koopman@ncmls.ru.nl.

Running title: Regulation and quantification of mitochondrial morphology and content.

Word count: 15,454 (total)
Characters: 107,091 (including spaces); 92,067 (excluding spaces)

Keywords: mitochondrial biogenesis, mitochondrial dynamics, mitochondrial degradation, living cells, TMRM, microscopy, segmentation, image analysis.

ABSTRACT

Mitochondria play a key role in signal transduction, redox homeostasis and cell survival, which extends far beyond their classical functioning in ATP production and energy metabolism. In living cells, mitochondrial content ("mitochondrial mass") depends on the cell-controlled balance between mitochondrial biogenesis and degradation. These processes are intricately linked to changes in net mitochondrial morphology and spatiotemporal positioning ("mitochondrial dynamics"), which are governed by mitochondrial fusion, fission and motility. It is becoming increasingly clear that mitochondrial mass and dynamics, as well as its ultrastructure and volume, are mechanistically linked to mitochondrial function and the cell. This means that proper quantification of mitochondrial morphology and content is of prime importance in understanding mitochondrial and cellular physiology in health and disease. This review first presents how cellular mitochondrial content is regulated at the level of mitochondrial biogenesis, degradation and dynamics. Next we discuss how mitochondrial dynamics and content can be analyzed with a special emphasis on quantitative live-cell microscopy strategies.

1. INTRODUCTION

Mitochondria house enzyme systems for β-oxidation of fatty acids, the tricarboxylic acid (TCA) cycle, ketogenesis and oxidative phosphorylation (OXPHOS) and as such are key generators of cellular energy in the form of ATP [1-3]. In addition, this organelle plays an important role in the physiology of mammalian cells through its involvement in reactive oxygen species (ROS) generation, calcium homeostasis, heat generation and apoptosis induction (see [4, 5] and the references therein). Structurally, mitochondria consist of an outer membrane (MOM) that surrounds the inner membrane (MIM). The MIM is highly folded ("cristae") and encloses the matrix compartment where metabolic enzymes and the mitochondrial DNA (mtDNA) reside [6-9]. ATP is produced via the combined action of the four MIM-embedded complexes (CI-CIV) of the electron transport chain (ETC) and by the MIM-embedded complex V (CV or the F_oF_1-ATPase) through a chemiosmotic coupling mechanism [3, 9, 10]. Together, CI-CV constitute the oxidative phosphorylation (OXPHOS) system, the proper functioning of which critically depends on the functional and structural integrity of MIM protein and lipid components. Given their role in numerous cellular pathways, it is not surprising that dysfunction of mitochondria is observed in many human pathologies. In principle, there are only two categories of mitochondrial diseases [4]: primary disorders (in which one of the 1200-1500 genes encoding a mitochondrial protein is mutated) and secondary disorders (where mitochondria are dysfunctional for a different reason). In this sense, (progressive) mitochondrial dysfunction has not only been linked to (relatively rare) metabolic disorders but also to normal human aging, neurodegeneration, cancer, diabetes and metabolic syndrome (*e.g.* [4, 5, 11-16]). Although mitochondria display a certain genetic and metabolic autonomy, their function is intricately linked to cellular physiology at the level of ion/metabolite exchange and (retrograde) signaling cascades [10, 17]. In addition, the cellular environment normally supplies mitochondria with (submaximal) substrate concentrations and sustains and controls mitochondrial (ultra)structure and motility ("mitochondrial dynamics). We and others therefore argued that mitochondrial (patho)physiology, if possible, should be studied in living cells, tissues and organisms (see [4, 5] and the references therein). During the last decade it has become increasingly clear that mitochondrial (dys)functioning, amount, (ultra)structure and subcellular positioning are tightly interconnected (*e.g.* [18-23]). Furthermore, the functional roles of mitochondria in metabolism and signaling appear to depend on the physical compartmentalization, subcellular localization and motility of the organelles, and *vice versa*. Clearly, changes in mitochondrial motility, fission and fusion

dynamics coincide with phenomena such as bioenergetic adaptation, cellular stress, autophagy and cell death, as well as pathological mechanisms involving mitochondrial dysfunction [24]. Moreover, mitochondrial morphology and mass can be modulated by various pharmacological treatments (**Table 1**). This has made the topics of mitochondrial dynamics, cellular mitochondrial content and its regulation subjects of intense study. Below, we summarize the current insights into how mitochondrial content is regulated (**section 2**) and discuss experimental strategies to quantify mitochondrial content (**section 3**).

2. REGULATION OF MITOCHONDRIAL CONTENT

One of the main purposes of mitochondria is to provide energy-consuming processes with an adequate supply of ATP. However, under certain conditions, cellular energy demands may exceed the mitochondrial capacity of ATP production, causing mild or severe energy depletion ("energy crisis"). This may either be the result of increased energy expenditure such as with endurance training, or due to a functional mitochondrial defect or mutation, relevant during pathological conditions. During energy crisis, ATP deficiency and/or mitochondrial dysfunction will activate adaptive mechanisms attempting to counterbalance this situation [23, 24, 42-44]. These interlinked regulatory systems control mitochondrial content at the transcriptional and functional level by modulating mitochondrial biogenesis/degradation, fission/fusion dynamics, motility and/or respiration [23]. Of note, mitochondrial content modulation might not work identically in the various cell types because of their different biological function and mitochondrial morphology (**Fig. 1**). This is compatible with the observation that mitochondrial abundance and expression levels of OXPHOS complexes apparently correlate with tissue- and cell-specific requirements of oxidative ATP generation [45, 46]. Below, we briefly discuss the three levels of regulation affecting mitochondrial content in more detail (**Fig. 2**): (**i**) regulation of mitochondrial biogenesis, (**ii**) regulation of mitochondrial degradation, (**iii**) regulation of mitochondrial dynamics.

2.1. MITOCHONDRIAL BIOGENESIS

Mitochondrial biogenesis can be defined as division and/or "growth" (*e.g.* elongation by fusion) of pre-existing mitochondria, serving to increase or replenish mitochondrial biomass [47]. Under physiological conditions, this process is an important adaptive mechanism to accommodate metabolic changes or energy depletion since it increases mitochondrial mass and, as a consequence, mitochondrial bioenergetic capacity. Biogenesis is observed after

endurance exercise, cold exposure and caloric restriction but also during conditions of oxidative stress and throughout cell division and differentiation [42, 46, 48-51]. Furthermore, thyroid hormones are known to increase metabolic rate and mitochondrial enzyme levels in rats [52], and both pre- and postnatal changes in mitochondrial biogenesis have been documented [53-55]. For instance, during embryonic development energy metabolism and mitochondrial (ultra)structure are remodeled in parallel [56]. At the early stage of embryogenesis (embryonic day 1), the zygotes contain spheroid mitochondria and depend on OXPHOS after which anaerobic glycolysis gradually takes over and reaches a maximum level following implantation. After this, glycolytic ATP generation becomes progressively less important because mitochondrial biogenesis is triggered and OXPHOS is reinitiated due to vascularization. Mitochondrial biogenesis is generally considered as a long-term adaptive response and not a transient accommodation to short fluctuations in energy supply. The latter can be met by enhancing mitochondrial capacity via posttranscriptional regulation (*e.g.* phosphorylation, (de)acylation, oxidative modification) and/or expression regulation of only a subset of mitochondrial proteins (*e.g.* [57-59]). In case of genetic mitochondrial disorders, increased mitochondrial biogenesis in skeletal muscle can be diagnostically observed as "ragged red fibres" [60]. In humans, about 1000 genes encoding mitochondrial proteins have been identified (MitoCarta human inventory, Broad Institute). The majority of these genes is located on the nuclear DNA (nDNA) since only 13 of them (all encoding subunits of the OXPHOS system) originate from mtDNA. Nuclear-encoded mitochondrial proteins are guided to their correct location in the outer or inner membranes, the inter membrane space or the matrix (for details see [61] and the references therein). This means that mitochondrial biogenesis requires an intricate control network of transcriptional regulators to properly orchestrate the coordinated expression of mtDNA and nDNA-encoded mitochondrial proteins during mitochondrial biogenesis [58, 62]. This information exchange is triggered by mitochondrial (dys)function, including alterations in MIM membrane potential ($\Delta\psi$), OXPHOS dysfunction and reduced mitochondrial and/or cytosolic ATP levels [63]. Controlling mitochondrial biogenesis not only involves nuclear-to-mitochondrial communication but also mitochondria-to-nucleus ("retrograde") signaling [64]. Directly below, we discuss the key proteins involved in transcriptional regulation of mitochondrial biogenesis (**Fig. 2**).

PGC-1α - One of the major players in mitochondrial biogenesis is the transcriptional coactivatior peroxisome proliferator-activated receptor gamma coactivator-1α (PGC-1α) [65, 66]. PGC-1α was first identified as a regulator of adaptive thermogenesis by regulating the expression of the mitochondrial uncoupling protein-1 (UCP-1) in brown fat [67]. Further research revealed that PGC-1α is highly expressed in mitochondria-rich tissues including heart and skeletal muscle [46, 68]. PGC-1α binds to, and regulates the activities of, several transcription factors and nuclear hormone receptors involved in mitochondrial biogenesis [65]. In this sense, PGC-1α coactivates nuclear respiratory factor-1 (NRF-1) [66], estrogen-related receptor alpha (ERRα) [69] and myocyte enhancer factor 2 (MEF2) [70]. Thereby it controls expression of several ETC and other mitochondrial proteins. In addition, PGC-1α is involved in fatty acid metabolism because it regulates peroxisome proliferator-activated receptors (PPARs) (for details see [42, 65] and the references therein).

NRF-1 - NRF-1 is a 68-kDa protein that is ubiquitously expressed in embryonic, fetal and adult tissues, with highest expression in skeletal muscle [47, 71]. It has a central DNA binding domain flanked by a nuclear localization signal and a transcriptional activation domain. NRF-1 binds to the recognition site in the target gene promoter region, as a homodimer, and activates transcription of the gene [72, 73]. NRF-1 DNA binding and trans-activation function is enhanced by serine phosphorylation of its N-terminal domain [74, 75]. NRF-1 recognition sites are found in in the proximal promoter of ubiquitously expressed genes [76], many of which are involved in mitochondrial biogenesis and metabolism [77]. Expression of a substantial number of nDNA-encoded OXPHOS genes has been linked to NRF-1 activity [78]. Moreover, NRF-1 has been found to regulate expression of key components of the mitochondrial protein import machinery, cytochrome *c*, and the rate-limiting enzyme in heme biosynthesis, 5-aminolevuline [79-81]. NRF-1 also regulates transcription factor A, mitochondrial (TFAM) [72], involved in transcription regulation of mtDNA-encoded genes and mitochondrial genome replication [82]. TFAM is required for the expression of the mitochondrial RNA polymerase (POLRMT) and the transcription factor B (TFB) regulators [83], two components of the mitochondrial transcription complex. Transcription of mitochondrial ribosomal proteins and tRNA synthases are also regulated by NRF-1 [84]. Genetic and biochemical analysis revealed that interactions between PGC-1α, NRF-1 and TFAM (co)control mitochondrial biogenesis and respiratory capacity [78]. Mitochondrial biogenesis stimulated by PGC-1α requires functional NRF-1, since a dominant negative NRF-

1 allele blocks the function of PGC-1 α [66]. The expression of both NRF-1 and PGC-1α has been found to be reduced in diabetes [85] and both factors have also been shown to be induced as a part of the adaptation of skeletal muscle to exercise training [86]. There are many other examples of mitochondrial content regulation via NRF-1 and associated mechanisms. For instance, NRF-1 and its downstream factor TFAM is upregulated in cells depleted of mtDNA and in rat hepatocytes following lipopolysaccharide treatment [87, 88]. In both of these model systems increased ROS levels were observed, suggesting that oxidative stress and/or redox changes might trigger mitochondrial biogenesis. It has also been suggested that NRF-1 might control the expression of ETC proteins in response to both extracellular signals and intracellular ATP concentrations [42]. With respect to the latter, another well described route of NRF-1-regulated mitochondrial biogenesis involves activation of AMP-dependent protein kinase (AMPK), a major sensor of cellular energy status [89-91]. AMPK is activated by AMP, which builds up during low energy (*i.e.* low ATP) conditions such as nutrient deprivation, physical exercise and/or bioenergetics dysfunction [92, 93]. AMPK activation in response to energy depletion stimulates expression of PGC-1α, triggering activation of NRF-1-mediated gene transcription [66, 94]. Interestingly, AMPK activation by the pharmacological agent 5-aminoimidazole-4-carboxamide riboside (AICAR) has been found to induce NRF-1 transcriptional activity through PGC-1α co-activation in various studies (*e.g.* [32, 95, 96]). The latter might explain the positive effects of AICAR in animal models of mitochondrial disease and fibroblast from patients with mitochondrial dysfunction [97, 98]. Upregulation of both NRF-1 and TFAM in skeletal muscle has also been associated with aging, suggesting that mitochondrial biogenesis is induced to compensate for mitochondrial functional deterioration [99].

NRF-2 - Another NRF family member, NRF-2, has also been found to regulate gene promoters of ETC subunits [100]. Occasionally, NRF-1 and NRF-2 recognition sites are present in the same promoter regions, suggesting that these factors act together in coordinating protein expression in relation to mitochondrial biogenesis (see [94] and the references therein).

PPARs **-** The PPAR family of ligand-activated transcription factors comprises several isoforms including PPARα, PPARβ and PPARγ [101]. These variants display different tissue-specific expression patterns and coordinate the expression of metabolic genes involved in

glucose and lipid metabolism [101, 102]. PPARs heterodimerize with the retinoid X receptor (RXR), and trans-activate target genes with compatible responsive elements in the promoter region encoding both mitochondrial and non-mitochondrial proteins. However, to the best of our knowledge, PPARs have not been directly associated with expression of ETC components [42]. PPARs are typically activated by long-chain fatty acids and their metabolites [103]. The PPARα isoform is expressed in cells with high rates of mitochondrial fatty acid oxidation, such as liver, heart, kidney and skeletal muscle, intestine and pancreas [101, 104]. The PPARβ isoform is ubiquitously expressed, and has been implicated in fatty acid oxidation as well as other mitochondrial processes [105, 106]. PPARγ is abundantly expressed in adipose tissue and at lower levels in skeletal muscle, liver, heart and bone marrow stromal cells, and regulates glucose metabolism and insulin sensitivity, and UCP-1-mediated thermogenesis [107].

ERRs - ERR transcription factors are involved in gene regulatory control networks involved in energy homeostasis, including fat and glucose metabolism as well as mitochondrial biogenesis and function [42, 108, 109]. Similar to PPARs and NRFs, ERRs are also co-activated by PGC-1α and expressed in tissues with high energy demands.

2.2. MITOCHONDRIAL DEGRADATION

Mitochondrial quality control occurs at the level of organelle and protein integrity and is carried out via mechanisms that identify the compromised components and marks them for destruction, followed by the subsequent recruitment of the machinery responsible for their degradation [11, 13, 110-113]. Quality control of mitochondrial proteins is described in detail elsewhere (*e.g.* [11, 114]**)**. The specific degradation of dysfunctional mitochondria ("mitophagy") is carried out by the lysosomal-autophagic machinery after the dysfunctional organelles have been marked for destruction. Key mediators of mitophagy include the PTEN (phosphatase and tensin homolog)-induced putative kinase 1 (PINK1), presenilin-associated rhomboid-like (PARL) protein and Parkin, a component of a multiprotein E3 ubiquitin ligase complex. PINK1 is normally located on the MOM, but is found at relatively low amount due to its continuous degradation by mitochondrial proteases [115-117]. Under conditions of (full) mitochondrial depolarization, this proteolytic activity is (fully) blocked leading to PINK1 accumulation on the MOM. When present at this location, PINK1 recruits cytoplasmic Parkin. This process therefore serves as a quality control mechanism for detecting and tagging

dysfunctional mitochondria, with low membrane potential, for degradation by mitophagy/autophagy. Interestingly, evidence was provided that Parkin also regulates the mitochondrial fission/fusion balance (see below) by ubiquitylation of fusion-promoting proteins (Mitofusins) on the MOM [118]. Mitochondrial fission is required to segregate dysfunctional mitochondria from the functional mitochondrial population and allow mitophagy. The current mechanism proposes that dysfunctional mitochondria have a (partially?) depolarized $\Delta\psi$ and, as a consequence, are trapped in autophagosomes for further lysosomal degradation. Mutations in the genes encoding PINK1 or Parkin have been implicated in early onset autosomal recessive Parkinson's disease, suggesting that mitochondrial quality control is of significance in this neurodegenerative pathology [119, 120]. Another protein involved in Parkinson's disease, α-synuclein, also appears to play a role in mitochondrial quality control. However, the nature of this involvement is currently not fully understood [121-123]. Obviously, mitochondrial biogenesis and degradation by mitophagy act antagonistically, but at the same time complementary; and together they determine net mitochondrial content and mitochondrial quality. However, experimental evidence suggests that mitochondrial biogenesis and autophagy are also more directly connected via the Parkin Interacting Substrate (PARIS) protein [124]. PARIS appears to be a repressor of PGC-1α by inhibiting its expression thereby inhibiting mitochondrial biogenesis. On the other hand, being a Parkin substrate, PARIS is degraded by the proteasome upon Parkin activation. A mechanism was proposed in which reduced Parkin expression/activity, as observed in Parkin-associated Parkinson's disease, leads to increased PARIS levels thereby affecting the balance between mitochondrial biogenesis and mitophagy [124]. Such a mechanism might amplify the negative effect of Parkin mutations on mitochondrial quality control [116]. In addition to the Pink1/Parkin system, several other proteins (*e.g.* valosin-containing protein (VCP), the p62 protein, microtubule-associated protein 1 light chain (LC3), the Bcl2/adenovirus E1B 19-kDa protein-interacting protein 3 (Bnip3), the mitochondrial voltage-dependent anion channel (VDAC) and the Nix protein) have been implicated in mitophagy induction, regulation and execution but these are discussed elsewhere [125-128].

2.3. MITOCHONDRIAL DYNAMICS

Mitochondrial morphology varies between different cell types, ranging from bean-shaped individual organelles to reticular structures (**Fig.1**). For example, in healthy rat hepatocytes mitochondria are evenly distributed throughout the cell and their structure is generally

spherical/ovoid (*e.g.* [129]). Mitochondrial reticular assemblies generally extend throughout the cytosol and are often closely juxtaposed to other cellular compartments like the nucleus and endoplasmic reticulum [130-132]. Mitochondrial morphology is, however, very dynamic and can shift between fragmented structures and tubular networks, via altering the balance between mitochondrial movement, fission and fusion events [133]. This balance determines the net morphology of the cellular mitochondrial population and is controlled by the activities of a growing set of "mitochondria-shaping" proteins (**Fig.2**; [134-143]). In mammals key proteins include mitofusin 1 (Mfn1) and mitofusin 2 (Mfn2), involved in MOM fusion; OPA1 (optic atrophy protein 1; MIM fusion), dynamin-related protein 1 (Drp1; MOM fission), and Fission protein 1 (Fis1; a Drp1-adaptor protein); and Miro and Milton (both involved in mitochondrial motility). At the posttranslational level, the activities of mitochondrial fusion/fission proteins is regulated by an collection of regulatory components (**Fig. 2**; details provided in [20, 143-148]). Interestingly, mitochondrial fusion and fission proteins also are directly involved in regulation of mitochondrial functional properties, strongly suggesting that mitochondrial shape, spatiotemporal localization and function are linked [135, 140, 149-155]. For instance, fragmentation and fusion events, and therefore also membrane remodeling, occurs both in response to metabolic influence and as part of cell death programs [135, 156, 157]. Moreover, Mfn2 loss-of-function inhibited pyruvate, glucose and fatty acid oxidation and induced mitochondrial depolarization [158]. In contrast, Mfn2 gain-of-function increased glucose oxidation and mitochondrial membrane potential. This suggests that Mfn2 (co)regulates mitochondrial function through a mechanism independent of its role in mitochondrial fusion. The mitochondrial volume fraction in the cell depends on the cell type and metabolic condition [159, 160]. In this sense, multiple mitochondrial abnormalities may be observed in muscle and skin cells of patients with inherited mitochondrial disorders (*e.g.* [161, 162]). Similarly, when mitochondrial function was chronically inhibited by rotenone, a specific blocker of the first ETC complex (CI), mitochondrial length and degree of branching dose-dependently increased [37, 163]. In the light of the above, and given the fact that mitochondrial shape and mass also can differ within and between the same cell type (*e.g.* [149, 150, 162]), a proper understanding of the relationship between mitochondrial content, shape and function requires statistical analysis. For this purpose functional and microscopy-based strategies have been developed, which are discussed in the following sections.

3. QUANTIFICATION OF MITOCHONDRIAL MORPHOLOGY AND CONTENT

Methods to evaluate mitochondrial function have been a topic of major interest in experimental research, pharmacological screening and clinical diagnostics. There are multiple experimental approaches to measure individual or composite mitochondrial properties. Common analyses include biochemical measurements of mitochondrial marker proteins and enzyme activities, quantitation of mtDNA level and fluorescence microscopy analysis [40, 45, 164, 165]. Also (cryo)-electron microscopy (EM) analysis of fixed specimens has been widely applied to analyze mitochondrial (ultra)structure (*e.g.* [41, 166-168]). As a consequence, morphometric analyses have been historically important to quantify mitochondrial properties using EM images [169]. New developments in the EM field, including tomography and image processing tools, have extended the analytic potential by enabling 3D-reconstruction, detection and segmentation of mitochondria, which has proven to be powerful methods to study mitochondrial internal and external structure. Additional information regarding EM analysis of mitochondrial (ultra)structure can be found elsewhere [170-180]. Below we discuss three other methodological approaches to assess mitochondrial morphology and/or content in biological samples: (**i**) bioenergetic capacity, (**ii**) biochemical biomarkers, and (**iii**) fluorescence microscopy analysis.

3.1. MITOCHONDRIAL BIOENERGETIC CAPACITY

Quantification of oxygen consumption rates is frequently used to assess mitochondrial oxidative capacity and thereby mitochondrial content in isolated mitochondria and (permeabilized) cells and tissue samples (*e.g.* [38-40, 181-185]). The strategy of isolating mitochondria from human and animal tissue/cell material has historically been very important, and the technique was pioneered by scientists such as Chance and Williams [186]. Analysis of mitochondria-enriched fractions led to the formulation of Mitchell's chemiosmotic theory [3] and the subsequent elucidation of other mitochondrial metabolic pathways like the TCA cycle [187]. Currently, optimized protocols for mitochondrial isolation from a variety of tissues and cells are available (*e.g.* [188, 189]). However, isolated mitochondria are relatively fragile and their morphology and function differs with that observed in living cells [190]. The latter relates to the fact that *in situ* mitochondrial function is closely linked to cell metabolism and associated with submaximal rates of mitochondrial enzyme activity. Moreover, as explained above, the cellular environment mediates communication between mitochondria the cytosol and other organelles during forward and retrograde mitochondrial signaling [154]. This means that data obtained with mitochondria-

enriched fractions is not necessarily informative about mitochondrial (patho)physiology at the cellular and tissue level. To overcome some of the adverse effects caused by the isolation procedure, permeabilization of the cellular membrane has been used as an alternative procedure to access mitochondrial activities. Using this method, mitochondrial function can be studied without dislocating the organelles from the intracellular compartment, and the metabolic conditions and substrate concentrations can still be controlled [181, 191]. However, the nature and significance of mitochondrial changes taking place during subcellular isolation is still under debate [192].

3.2. BIOCHEMICAL BIOMARKERS

Another common method to determine mitochondrial content involves analysis of the protein levels of (a collection of) mitochondrial proteins such as OXPHOS subunits and/or membrane transporters in cell or tissue lysates (*e.g.* [25, 40]). Similarly, analysis of individual enzyme activities under non-substrate limiting (Vmax) conditions generally reflects the levels of mitochondrial OXPHOS proteins (*e.g.* [193]). Indeed, analysis of cells from patients with isolated CI deficiency, maximal CI enzymatic activity and the amount of fully-assembled CI (determined by native gel electrophoresis) proportionally declined [194]. However, mitochondrial content was not reduced in these cells [150], demonstrating that OXPHOS protein levels and Vmax values not always reflect mitochondrial content. An alternative strategy to analyze mitochondrial biogenesis and content involves quantification of mRNA levels of nDNA-encoded genes of OXPHOS subunits and mitochondrial transcription regulators (*e.g.* [40, 183]). Furthermore, recent progress in real-time quantitative PCR technology has enabled sensitive analysis of mtDNA copy number in small sample volumes [195]. By this method mtDNA content is quantified relative to nDNA, yielding a mitochondrial-to-nuclear DNA ratio as measure of mtDNA copy number, which was used as a measure of mitochondrial content in animal and clinical studies [40, 196-198]. It should, however, be mentioned that changes in OXPHOS protein expression or mtDNA levels do not always correlate with changes in mitochondrial content (*e.g.* [199, 200]). The expression level and/or the activity of citrate synthase, a mitochondrial matrix enzyme, is commonly used as a reference when evaluating relative changes in mitochondrial properties or as a surrogate marker of total mitochondrial volume and content (*e.g.* [193]). The protein amount of several marker enzymes can also be evaluated using histochemical staining of tissue preparations,

including nicotinamide adenine dinucleotide tetrazolium reductase [201], cytochrome *c* oxidase [202] and succinate dehydrogenase [203, 204].

3.3. FLUORESCENCE MICROSCOPY

Microscopy techniques have been essential in mitochondrial research since the discovery of these organelles back in the 1840's [205]. Nowadays, mitochondrial analysis by live-cell microscopy represents the most direct method to retrieve authentic information about mitochondrial shape, position and content. Development of superresolution microscopy techniques has allowed imaging of fluorescently labeled cells and organelles at unprecedented levels of resolution [206-212]. For example, using three-dimensional (3D) structured-illumination microscopy (SIM) resolution was doubled relative to a wide-field fluorescence microscope yielding values of 120 nm (lateral) and 360 nm (axial). The SIM approach allowed live-cell recordings of mitochondrial (ultra)structure in living cells at up to 5 s per volume for >50 time points [213].

Visualization of mitochondria by live-cell microscopy - Mitochondria in living cells are generally visualized using chemical and/or proteinaceous fluorescent reporter molecules ("probes"; **Fig. 1**; [214, 215]). Chemical probes can be introduced into the cells using specific incubation protocols whereas protein-based probes require cell transduction or transfection. Alternatively, (inducible) cell lines can be created that stably express the protein-based probe of interest (*e.g.* [21, 216-218]). For chemical probes mitochondrial targeting often depends on the fact that mitochondria possess a high inside-negative membrane potential ($\Delta\psi$). This means that (positively charged) lipophilic cations accumulate in the mitochondrial matrix in a $\Delta\psi$-dependent manner according to the Nernst-equation [219]. Often used cations include rhodamine-123 (R123), tetramethylrhodamine methyl ester (TMRM), tetramethylrhodamine ethyl ester (TMRE) and 5,5',6,6'-tetrachloro-1,1',3,3'-tetraethylbenzimidazolyl-carbocyanine (JC-1). When accompanied by proper control experiments (see [219, 220] and the references therein), the mitochondrial fluorescence signal of the above cations constitutes a measure of $\Delta\psi$. At sufficiently negative $\Delta\psi$, JC-1 monomers (green fluorescence) accumulate in the mitochonrial matrix to such extend that J-aggregates are formed (red fluorescence), allowing ratio-metric analasis of $\Delta\psi$. Several non-cationic chemical probes (*e.g.* members of the "mitotracker" family) react with mitochondrial constituents, thereby trapping them in the matrix and rendering their mitochondrial localization less $\Delta\psi$ dependent. Protein-based

mitochondria-targeted probes generally consist of a mitochondrial targeting-sequence that is N-terminally fused to a (spectral variant of the) green fluorescent protein (mitoGFP). Using routine equipment, wide-field fluorescence microscopy allows acquisition of two-dimensional (2D) images of cells whereas confocal microscopy enables acquisition of three-dimensional (3D) image data-sets (z-stacks). In principle, both types of microscopy allow time-lapse studies although 3D image acquisition should be fast enough to prevent mitochondrial movement artifacts within individual z-stacks. The latter problem is minimized by measuring at 20^{o}C (instead of 37^{o}C) thereby reducing mitochondrial motility. Alternatively, a spinning-disk confocal microscope can be used, which allows more rapid 3D data acquisition. Live-cell microscopy in combination with mitochondria-selective probes can be employed for high-content strategies to simultaneously assess multiple mitochondrial functional properties (*e.g.* $\Delta\psi$), motility, morphology, mass and position [5, 160, 221-223]. However, visual inspection and/or manually categorizing of these images will not permit unbiased and quantitative analysis of mitochondrial parameters.

Quantification of mitochondrial morphology and content using image analysis **-** With respect to mitochondrial content, the fractional cellular volume occupied by mitochondria has been measured based on fluorescence detection of mitoGFP and calcein blue in the cytosol [224]. Alternatively, we and others have developed procedures allowing systematic analysis of mitochondrial shape, number and mass using fluorescence microscopy images (**Table 2**). This can be carried out using for example the freely available Fiji (http://pacific.mpi-cbg.de/wiki/index.php/Main_Page) or OpenCV software (www.opencvb.org) or commercial programs like Matlab (www.mathworks.com) or Image Pro Plus (www.mediacy.com). Automated methods generally apply an image processing algorithm ("pipeline"; **Fig. 3A**), which involves highlighting the position of mitochondrial structures by generation of a binary (BIN) image (segmentation), followed by masking of the background-corrected original image (COR) using this BIN image. From the BIN image (representing white mitochondrial objects on a black background) various mitochondrial parameters ("descriptors") can be extracted. These descriptors include the number of mitochondria per cell (*Nc*), the mean area of individual mitochondria (*Am*), the mitochondrial mass (which can be approximated in cells with a relatively flat morphology by the product of *Nc* and *Am*; [219, 222] or by summing up all values of Am within a given cell), mitochondrial aspect ratio (*AR*, a measure of mitochondrial length) and mitochondrial formfactor (*F*, a combined measure of mitochondrial

length and degree of branching; [37, 149]). In principle, when combined with an automated high-throughput microscopy system the above pipeline allows for automated high-content, high-throughput, screening [4, 5, 254]. To illustrate our quantitative approach we segmented the mitochondria for various images depicted in **figure 1**. Visual inspection of the resulting BIN images (**Fig. 3B**) reveals that the above processing pipeline, originally developed for R123-stained primary human skin fibroblasts [37, 222], gave correct results for 7 out of 10 conditions (**Fig. 3C**, green bars). However, mitochondrial segmentation was not successful in panels Bh, Bn and Br, thereby yielding erroneous values for *Nc*, *Am*, mitochondrial mass, *AR* and *F* (**Fig. 3C**, red bars). This means that prior to implementation of automated processing and quantification, a pipeline should be manually validated for the given cell type by visual inspection. Once the experimental conditions for successful automated quantification have been established for a certain cell type, images yielding erroneous descriptor values can be automatically identified and discarded from the analysis by comparing their descriptor values with the cell population average. The above results clearly demonstrate that a certain experimental strategy (*e.g.* cell type, mitochondrial probe, microscopy hardware, image acquisition procedure) requires a tailor-made processing/analysis pipeline (and *vice versa*). Crucially, it is important to realize that image magnification/resolution (*i.e.* the used microscopy objective) and signal-to-noise (S/N) ratio need to be compatible with the size of the (small) mitochondrial objects and the to-be designed processing protocol [37, 162, 222]. As an example of quantification of mitochondrial content (*i.e.* mass) in 2D microscopy images, we have previously developed a high-content strategy for primary human skin fibroblasts [220, 222]. Mitochondrial mass in these cells can be approximated by multiplying the number of mitochondria per cell (*Nc*) by the mean mitochondrial area (*Am*) of the mitochondrial objects. This strategy is particularly applicable to fibroblasts and other cell types with a flat morphology since in this case the lateral cell dimensions (area) greatly exceed its axial dimensions (height). Under these conditions the total mitochondrial volume can be approximated by the total mitochondrial area (*i.e.* the product of *Nc* and *Am*). To demonstrate the application of this approach we investigated the effect of changes in cellular metabolic state on mitochondrial shape and mass. Therefore healthy primary skin fibroblasts were cultured for 24 h in normal glucose-containing medium (GLU) and medium in which the glucose was replaced by galactose (GAL) and dialyzed serum was used (**Fig. 4**). In cancer cells, this maneuver shifts energy metabolism from glycolysis towards OXPHOS-mediated ATP generation [255]. Visual comparison of typical live-cell microscopy images suggests that

GAL treatment induces mitochondrial fragmentation (**Fig. 4A** *vs.* **Fig.4B**). Image segmentation based upon *Am* [219] followed by visual inspection suggests that mitochondria become smaller in GAL-treated cells (**Fig. 4C**). A more complete analysis for a population of cells revealed that GAL treatment does not affect *Nc*, but significantly reduces *Am*, mitochondrial mass, *AR* and *F*. These results suggest that 24 h GAL treatment does not induce mitochondrial fragmentation (*i.e. Nc* is not affected) but leads to mitochondrial shrinkage and a reduced mitochondrial mass. However, since we used a $\Delta\psi$-dependent R123 staining for mitochondrial visualization, we cannot rule out that GAL treatment induces $\Delta\psi$ depolarization to such extent that mitochondria are "missed" in the analysis. Importantly, the reliability of using the product of *Am* and *Nc* as a measure of mitochondrial mass also depends on cell size. This is caused by the fact that larger cells generally contain more and larger mitochondrial objects. For instance, in the case of primary skin fibroblasts from patients with isolated CI deficiency we analyzed 2D images of cells stained with CM-DCF (chloromethyl-2',7'-dichlorofluorescein; see [256] for protocol). This ROS probe is localized in the cytosol and revealed that control cells have a size of 100±15% (N=27 cells; CT5120 cell line) whereas a size of 183±15% (N=19) was found in a patient cell line (P5171). Similarly, mitochondrial mass in P5171 cells was 194% of that in CT5120 cells (**Fig. 5A, Fig. 5B**), demonstrating that mitochondrial mass measurements should be accompanied by cellular size quantification. If fluorescent cations are used for mitochondrial staining, some fluorescence signal might be originating from the cytosol leading to a distinct peak in the intensity histogram (**Fig. 5C**). In this case, image processing can be used to segment the cytosolic compartment using thresholding (T) and median filtering (MED; **Fig. 5D**). Superposition of the mitochondrial BIN image (**Fig. 5B**) and cytosolic MED image using a Boolean "AND" operation (similar to **Fig. 3A**), can then be used to calculate the mitochondrial mass corrected for cellular size (*i.e.* the ratio between the total mitochondrial area from the BIN image and the total cytosolic area from the MED image). The result of this procedure (**Fig. 5D**; "BIN *AND* MED" image) depicts mitochondria (light blue) within the cytosol (dark blue).

Interpretation of quantitative data for mitochondrial morphology and content in 2D microscopy images – In case of primary skin fibroblasts from patients with isolated CI deficiency, we observed that individual mitochondria appeared fragmented and/or less branched in patient fibroblasts with a severely reduced CI amount and activity (class I), whereas patient cells in which these latter parameters were only moderately reduced displayed

a normal mitochondrial morphology (class II; [150]). Comparing these mitochondrial morphology alterations with other cellular and mitochondrial readouts revealed that, relative to class II patients, class I patients displayed an earlier age of disease onset and death, a larger reduction in CI enzymatic activity, a greater increase in NADH/ROS levels and lower cellular levels of OXPHOS proteins [257]. With respect to ROS signaling, we provided evidence that mitochondrial morphology and function are controlled by endogenous ROS and redox signaling [38, 228]. A recent conceptual model [20, 148] proposes that mitochondria can exist in three morphological "states" of net morphology: (**i**) a filamentous or "hyperfused" state, (**ii**) an intermediate or "normal" state, and (**iii**) a fragmented state (**Fig. 6A**). These morphologies have been linked to distinct cellular and mitochondrial metabolic states and conditions, supporting the model that mitochondrial function determines mitochondrial morphology and *vice versa* [20, 148, 258-260]. Each of the three morphological states was associated with a distinct phenotype of mitochondrial parameters in primary human skin fibroblasts (**Fig. 6B**). Combining this multivariate dataset with its associated "biological" meaning (**Fig. 6C**) allowed correct classification of the observed phenotypes. Of note, using multiple mitochondrial parameters allows not only for identification of "classical" filamentous and fragmented morphologies but also is able to identify mitochondrial elongation, shrinkage, biogenesis and increased fusion/fission (**Fig. 6C**).

3D analysis of mitochondrial morphology and content **-** Automated quantification of mitochondrial morphology and content has been most successful using wide-field or confocal 2D images (**Table 2**). For reasons explained above this strategy is less applicable to thicker specimens [222]. However, a "semi-3D" image can be created by collapsing multiple image-sections from a wide-field or confocal z-stack into a single 2D projection [224, 261]. A more advanced strategy consists of calculating a 3D representation of the mitochondrial compartment from the z-stack and performing a 3D analysis of mitochondrial number, morphology (*e.g.* sphericity) and content (*e.g.* total volume). Although the technical requirements for image acquisition, processing and analysis are significantly more demanding than for 2D procedures, recent attempts to analyze mitochondria in 3D have demonstrated that this strategy has promising potential [247]. The latter study as well as others (*e.g.* [249]) demonstrated that additional mitochondrial subtyping (*i.e.* using more than the three categories described above) may also be applied to account for differences in shape and appearance. Thus, the descriptors to be analyzed should depend on the physiological or

experimental context in the particular study, and whether it is the mitochondrial fragmentation state or other shape changes that are of interest.

4. SUMMARY AND CONCLUSIONS

Until recently, changes in mitochondrial content were explained primarily in terms of mitochondrial biogenesis or proliferation, without accounting for removal of damaged organelles. However, the cellular mitochondrial content under a given condition results from the balance between mitochondrial biogenesis, dynamics and degradation. Since mitochondria represent primary sites of both metabolism and cell signaling, they serve as sensors, effectors, and executors in various physiological processes to accommodate contextual influences. This includes adaptive responses to re-establish a new steady state situation for the cell, or cell death if the effects are severe and vital physiological thresholds are crossed. The mitochondrial responses are thus manifold, and serve to balance metabolic and energetic needs in the cell. Therefore studies of mitochondrial content cannot be completely dissociated from the physiological cellular context that (co)determines an observed mitochondrial content change. This means that interpretation of the obtained data needs to consider at least two major questions in order to evaluate the potential effects on mitochondrial physiology: (**i**) To what extent does the observed results reflect, or relate to, the authentic physiological context in a viable cell or tissue? (**ii**) Is it possible that the observed effect is reciprocally balanced or compensated by other mechanisms in the cell (adaptation)? Although, "mitochondrial number" still might represent a useful descriptor for some applications and tissues, it does not properly reflect the content of mitochondrial biomass since it depends on the specificities of mitochondrial morphology and size, and phenomena such as fusion and fission. Therefore computer-assisted 2D and 3D analysis of live-cell microscopy images provides a promising strategy for quantification and statistical analysis of mitochondrial shape and content in an unbiased manner. However, experimental conditions and the used cell type should be compatible with the applied quantification approach and not be applied without a proper understanding of the biology involved and potential pitfalls.

ACKNOWLEDGEMENTS

This work was supported by equipment grants of ZON (Netherlands Organization for Health Research and Development, No: 903-46-176), NWO (Netherlands Organization for Scientific

Research, No: 911-02-008), and by the CSBR (Centres for Systems Biology Research) initiative from the Nederlandse organisatie voor Wetenschappelijk Onderzoek (NWO, Netherlands Organisation for Scientific Research, Grant: #CSBR09/013V). The work was also supported by grants of NFR (Norwegian Research Council, No: 214187/F20) and BMFS (Bergen Medical Research Foundation). We are grateful to Dr. F. van Kuppeveld (Dept. of Medical Microbiology, RUMC, Nijmegen) for providing the BGM cells, Ing. S.E. van Emst-de Vries (Dept. of Biochemistry, RUMC) for isolating primary rat pancreatic acinar cells and culturing of CHO cells, Ing. A. Oosterhof (Dept. of Biochemistry, RUMC) for human myoblast and myotubes culture, Dr. J.W. Kuiper (Dept. of Cell Biology, RUMC) for providing primary mouse hippocampal neurons and glia cells, Dr. F. Valsecchi for providing primary mouse skin fibroblast and Ing. H. Swarts (Dept. of Biochemistry, RUMC) for practical assistance in developing the protein-based fluorescent probes.

ABBREVIATIONS

$\Delta\psi$, mitochondrial membrane potential
AICAR, 5-aminoimidazole-4-carboxamide riboside
Am, the area of individual mitochondris
AMPK, AMP-dependent protein kinase
AR, mitochondrial aspect ratio
BIN, binary image
BNIP3, Bcl2/adenovirus E1B 19-kDa protein-interacting protein 3
CM-DCF, chloromethyl-2',7'-dichlorofluorescein
COR, background-corrected microscopy image
Drp1, dynamin-related protein 1
EM, electron microscopy
ERRα, estrogen-related receptor alpha
ETC, electron transport chain
F, mitochondrial formfactor
Fis1, fission protein 1
GFP, green fluorescent protein
JC-1, 5,5',6,6'-tetrachloro-1,1',3,3'-tetraethylbenzimidazolyl-carbocyanine
MIM, mitochondrial inner membrane
MED, median (filtered) image
MEF2, myocyte enhancer factor 2
Mfn1/2, mitofusin 1/2
MOM, mitochondrial outer membrane
mtDNA, mitochondrial DNA
Nc, number of mitochondria per cell
nDNA, nuclear DNA
NRF-1, nuclear respiratory factor-1
NRF-2, nuclear respiratory factor-2
OPA1, optic atrophy protein 1
OXPHOS, oxidative phosphorylation
PARIS, parkin interacting substrate

PARL, presenilin-associated rhomboid-like
PGC-1α, peroxisome proliferator-activated receptor gamma coactivator-1α
PINK1, PTEN (phosphatase and tensin homolog)-induced putative kinase
POLRMT, mitochondrial RNA polymerase
PPAR, peroxisome proliferator-activated receptor
R123, rhodamine 123
ROS, reactive oxygen species
RXR, retinoid X receptor
SIM, structured-illumination microscopy
S/N, signal-to-noise
T, thresholding, thresholded
TCA, tricarboxylic acid cycle
TFAM, Transcription factor A, mitochondrial
TFB, transcription factor B
TMRE, tetramethylrhodamine ethyl ester
TMRM, tetramethylrhodamine methyl ester
UCP-1, uncoupling protein-1
VCP, valosin-containing protein
VDAC, voltage-dependent anion channel

FIGURE LEGENDS

Figure 1: Mitochondrial morphology in various cell types. Mitochondria were visualized by live-cell microscopy in the indicated cell types using either a chemical (*i.e.* JC1, MR, R123, TMRM) or a protein-based reporter molecule (mitoEYFP). The scale bar equals 15 µm. (**A**) Primary human myoblast (HM) stained with rhodamine 123 (R123). (**B**) Primary mouse myoblast (MM) stained with Mitotracker Red CMXRos (MR). (**C**) Primary human skin fibroblast (HSF) stained with tetramethylrhodamine ethyl ester (TMRM). (**D**) Primary mouse skin fibroblast (MSF) stained with R123. (**E**) Primary mouse hippocampal glia cell (MHG) stained with R123. (**F**) Primary mouse hippocampal neuron (MHN) stained with R123. (**G**) Primary rat pancreatic acinar cells (RPAC) stained with R123. (**H**) Primary human myotubes (HMT) stained with 5,5',6,6'-tetrachloro-1,1',3,3'-tetraethylbenzimidazolyl- carbocyanine (JC-1). (**I**) Buffalo Green Monkey kidney (BGM) cells expressing mitochondria-targeted enhanced yellow fluorescent protein (mitoEYFP). (**J**) Primary human skin fibroblast (HSF) expressing mitoEYFP. (**K**) Primary human myotubes (HMT) expressing mitoEYFP. (**L**) Chinese Hamster Ovary (CHO) cells expressing mitoEYFP.

Figure 2: Regulation of mitochondrial biogenesis, dynamics and degradation in mammalian cells. Mitochondrial content depends on the cell-controlled balance between mitochondrial biogenesis (activated by endogenous or exogenous signals), mitochondrial degradation and mitochondrial dynamics. The latter is controlled by a variety of regulatory signals (see **Section 2** in the main text for details).

Figure 3: Quantification of mitochondrial morphology in selected cell types. (**A**) Image processing and analysis flow scheme for quantification of mitochondrial morphology parameters in living cells. A fluorescent reporter molecule is used to specifically visualize mitochondria and a microscopy image is taken. This image (RAW) is background-corrected (BC) to yield the COR image. The latter image is subsequently processed by a linear contrast stretch (LCS) operation, a top-hat filter (THF), a median filter (MED) and thresholded (T) to yield a binary (BIN) image. The BIN image highlights white mitochondrial objects on a black background. Combination of the BIN and COR image using a Boolean "AND" operation allows calculation of a masked image (MSK) and calculation of fluorescence intensity information for each mitochondrial object. (**B**) Calculation of the BIN image for a variety of

cell types (live-cell images were taken from **figure 1**) by applying the algorithm in panel A. (**C**) Parameters extracted from the BIN images: calculation of the number of mitochondrial objects per cell (*Nc*), the mean area of each individual mitochondrial object (*Am*), mitochondrial mass (calculated by taking the product of *Nc* and *Am*, the mean mitochondrial object aspect ratio (*AR*, a measure of mitochondrial length) and the mean mitochondrial object formfactor (*F*, a combined measure of mitochondrial length and degree of branching). In this panel, the designation of the corresponding binary image in panel B is given on the x-axis. Not all binary images in panel B yielded correct results. Reliable data are represented by green columns; incorrect data is represented by red columns. Data obtained using a different magnification is indicated by #. Error bars represent standard error of the mean (SEM).

Figure 4: Mitochondrial shrinkage and content reduction visually resemble mitochondrial fragmentation. Mitochondrial morphology was analyzed in R123-stained primary human skin fibroblasts from a healthy volunteer (CT5120). These cells were cultured in normal medium containing 5.5 mM glucose (GLU) and in the same medium without GLU but with 5.5 mM galactose (GAL) and dialyzed serum for 24 h. (**A**) Typical COR and BIN image (see **figure 2** and main text for details about the image processing) of cells cultured in GLU-containing medium. (**B**) Similar as panel A but now for cells cultured in GAL-containing medium. (**C**) Segmentation of differently-sized mitochondria for the GLU (panel A) and GAL (panel B) condition based upon their area (*Am*) from large (>1000) to small (10-20). (**D**) Average values of *Nc*, *Am*, mitochondrial mass, *AR* and *F* (see **figure 2** and main text for the meaning of these parameters) for GLU and GAL conditions in a number (N) of cells.

Figure 5: Mitochondrial mass and relevance of cell size. (**A**) Typical RAW and BIN image (see **figure 2** for details about the image processing) of TMRM-stained primary human skin fibroblasts from a healthy volunteer (CT5120). The integrated optical density in the BIN image divided by 2, which is proportional to the total number of mitochondrial pixels in a single cell, equaled 2094190. (**B**) Similar to panel A but now for fibroblast from a patient with mitochondrial disease due to an isolated mitochondrial complex I deficiency (P5171; [262]. Here the integrated optical density in the cell equaled 4056290 (*i.e.* 194% of CT5120 cells). (**C**) Intensity histogram and magnification (inset) of the RAW image in panel B. Using a threshold value of 16 (gray value) allows segmentation of the cytosolic compartment (see also panel D). (**D**) Calculation of the cytosolic area using the RAW image in panel B. Following a

threshold operation (T), the image is median-filtered (MED; 3x3 filter size, 3 times) and combined with the BIN image in panel B using a Boolean "AND" operation (BIN *AND* MED). The latter figure depicts mitochondria (light blue) within the cytosol (dark blue). The total number of mitochondrial pixels equaled 4056290 (*i.e.* 9.54% of the total number of cytosolic pixels equaling 42513000).

Figure 6: Functional consequences and quantification of mitochondrial morphology and mass alterations. (**A**) Binary (BIN) images obtained by image processing of microscopy images from primary human skin fibroblasts stained with R123. Cells were obtained from a healthy volunteer (CT5120; "filamentous" and "intermediate" panel) and a patient with isolated mitochondrial complex I deficiency (P6173: "Fragmented" panel). Mitochondrial and cellular conditions/properties associated with the filamentous and fragmented phenotypes are indicated. (**B**) Quantitative parameters extracted from the BIN images in panel A. Depicted are the number of mitochondrial objects per cell (*Nc*), the mean area of each individual mitochondrial object (*Am*), mitochondrial mass (calculated by taking the product of *Nc* and *Am*, the mean mitochondrial object aspect ratio (*AR*, a measure of mitochondrial length) and the mean mitochondrial object formfactor (*F*, a combined measure of mitochondrial length and degree of branching). Data was expressed as percentage of the average value obtained for cells with an intermediate mitochondrial morphology phenotype. (**C**) Classification scheme of mitochondrial morphology phenotypes using the parameters described in panel B.

REFERENCES

[1] Kennedy EP, Lehninger AL. Oxidation of fatty acids and tricarboxylic acid cycle intermediates by isolated rat liver mitochondria. J Biol Chem 1949; 179: 957-72.

[2] Chapman MJ, Miller LR, Ontko JA. Localization of the enzymes of ketogenesis in rat liver mitochondria. J Cell Biol 1973; 58: 284-306.

[3] Mitchell P. Coupling of phosphorylation to electron and hydrogen transfer by a chemi-osmotic type of mechanism. Nature 1961; 191: 144-8.

[4] Koopman WJ, Willems PH, Smeitink JA. Monogenic mitochondrial disorders. N Engl J Med 2012; 366: 1132-41.

[5] Koopman WJ, Distelmaier F, Smeitink JA, Willems PH. OXPHOS mutations and neurodegeneration. EMBO J 2013; 32: 9-29.

[6] Palade GE. The fine structure of mitochondria. The Anatomical record 1952; 114: 427-51.

[7] Palade GE. An electron microscope study of the mitochondrial structure. The journal of histochemistry and cytochemistry: official journal of the Histochemistry Society 1953; 1: 188-211.

[8] Nass MM, Nass S. Intramitochondrial Fibers with DNA Characteristics. I. Fixation and Electron Staining Reactions. J Cell Biol 1963; 19: 593-611.

[9] Smeitink J, van den Heuvel L, DiMauro S. The genetics and pathology of oxidative phosphorylation. Nat Rev Genet 2001; 2: 342-52.

[10] Koopman WJ, Nijtmans LG, Dieteren CE, Roestenberg P, Valsecchi F, Smeitink JA, Willems PH. Mammalian mitochondrial complex I: biogenesis, regulation, and reactive oxygen species generation. Antioxid Redox Signal 2010; 12: 1431-70.

[11] Fischer F, Hamann A, Osiewacz HD. Mitochondrial quality control: an integrated network of pathways. Trends Biochem Sci 2012; 37: 284-92.

[12] Nunnari J, Suomalainen A. Mitochondria: in sickness and in health. Cell 2012; 148: 1145-59.

[13] Rugarli EI, Langer T. Mitochondrial quality control: a matter of life and death for neurons. EMBO J 2012; 31: 1336-49.

[14] Schon EA, DiMauro S, Hirano M. Human mitochondrial DNA: roles of inherited and somatic mutations. Nat Rev Genet 2012; 13: 878-90.

[15] Smith RA, Hartley RC, Cocheme HM, Murphy MP. Mitochondrial pharmacology. Trends Pharmacol Sci 2012; 33: 341-52.

[16] Vafai SB, Mootha VK. Mitochondrial disorders as windows into an ancient organelle. Nature 2012; 491: 374-83.

[17] Palmieri F. Diseases caused by defects of mitochondrial carriers: a review. Biochim Biophys Acta 2008; 1777: 564-78.

[18] Detmer SA, Chan DC. Functions and dysfunctions of mitochondrial dynamics. Nat Rev Mol Cell Biol 2007; 8: 870-9.

[19] Benard G, Rossignol R. Ultrastructure of the mitochondrion and its bearing on function and bioenergetics. Antioxid Redox Signal 2008; 10: 1313-42.

[20] Westermann B. Mitochondrial fusion and fission in cell life and death. Nat Rev Mol Cell Biol 2010; 11: 872-84.

[21] Dieteren CE, Willems PH, Swarts HG, Fransen J, Smeitink JA, Koopman WJ, Nijtmans LG. Defective mitochondrial translation differently affects the live cell dynamics of complex I subunits. Biochim Biophys Acta 2011; 1807: 1624-33.

[22] Saxton WM, Hollenbeck PJ. The axonal transport of mitochondria. J Cell Sci 2012; 125: 2095-104.

[23] Jose C, Melser S, Benard G, Rossignol R. Mitoplasticity: adaptation biology of the mitochondrion to the cellular redox state in physiology and carcinogenesis. Antioxid Redox Signal 2013; 18: 808-49.

[24] Fulda S, Gorman AM, Hori O, Samali A. Cellular stress responses: cell survival and cell death. Int J Cell Biol 2010; 2010: doi: 10.1155/2010/214074.

[25] Jose C, Hebert-Chatelain E, Bellance N, Larendra A, Su M, Nouette-Gaulain K, Rossignol R. AICAR inhibits cancer cell growth and triggers cell-type distinct effects on OXPHOS biogenesis, oxidative stress and Akt activation. Biochim Biophys Acta 2011; 1807: 707-18.
[26] Wang X, Moraes CT. Increases in mitochondrial biogenesis impair carcinogenesis at multiple levels. Mol Oncol 2011; 5: 399-409.
[27] Medina DJ, Tsai CH, Hsiung GD, Cheng YC. Comparison of mitochondrial morphology, mitochondrial DNA content, and cell viability in cultured cells treated with three anti-human immunodeficiency virus dideoxynucleosides. Antimicrob Agents Chemother 1994; 38: 1824-8.
[28] Nisoli E, Falcone S, Tonello C, Cozzi V, Palomba L, Fiorani M, Pisconti A, Brunelli S, Cardile A, Francolini M, Cantoni O, Carruba MO, Moncada S, Clementi E. Mitochondrial biogenesis by NO yields functionally active mitochondria in mammals. Proc Natl Acad Sci USA 2004; 101: 16507-12.
[29] Lee HC, Yin PH, Lu CY, Chi CW, Wei YH. Increase of mitochondria and mitochondrial DNA in response to oxidative stress in human cells. Biochem J 2000; 348 Pt 2: 425-32.
[30] Perez-de-Arce K, Foncea R, Leighton F. Reactive oxygen species mediates homocysteine-induced mitochondrial biogenesis in human endothelial cells: modulation by antioxidants. Biochem Biophys Res Commun 2005; 338: 1103-9.
[31] Stetler RA, Leak RK, Yin W, Zhang L, Wang S, Gao Y, Chen J. Mitochondrial biogenesis contributes to ischemic neuroprotection afforded by LPS pre-conditioning. J Neurochem 2012; 123 Suppl 2: 125-37.
[32] Kukidome D, Nishikawa T, Sonoda K, Imoto K, Fujisawa K, Yano M, Motoshima H, Taguchi T, Matsumura T, Araki E. Activation of AMP-activated protein kinase reduces hyperglycemia-induced mitochondrial reactive oxygen species production and promotes mitochondrial biogenesis in human umbilical vein endothelial cells. Diabetes 2006; 55: 120-7.
[33] Cunningham JT, Rodgers JT, Arlow DH, Vazquez F, Mootha VK, Puigserver P. mTOR controls mitochondrial oxidative function through a YY1-PGC-1alpha transcriptional complex. Nature 2007; 450: 736-40.
[34] Csiszar A, Labinskyy N, Pinto JT, Ballabh P, Zhang H, Losonczy G, Pearson K, de Cabo R, Pacher P, Zhang C, Ungvari Z. Resveratrol induces mitochondrial biogenesis in endothelial cells. Am J Physiol Heart Circ Physiol 2009; 297: H13-20.
[35] Lagouge M, Argmann C, Gerhart-Hines Z, Meziane H, Lerin C, Daussin F, Messadeq N, Milne J, Lambert P, Elliott P, Geny B, Laakso M, Puigserver P, Auwerx J. Resveratrol improves mitochondrial function and protects against metabolic disease by activating SIRT1 and PGC-1alpha. Cell 2006; 127: 1109-22.
[36] Wilson-Fritch L, Burkart A, Bell G, Mendelson K, Leszyk J, Nicoloro S, Czech M, Corvera S. Mitochondrial biogenesis and remodeling during adipogenesis and in response to the insulin sensitizer rosiglitazone. Mol Cell Biol 2003; 23: 1085-94.
[37] Koopman WJ, Verkaart S, Visch HJ, van der Westhuizen FH, Murphy MP, van den Heuvel LW, Smeitink JA, Willems PH. Inhibition of complex I of the electron transport chain causes O2-. -mediated mitochondrial outgrowth. Am J Physiol Cell Physiol 2005; 288: C1440-50.
[38] Distelmaier F, Valsecchi F, Forkink M, van Emst-de Vries S, Swarts HG, Rodenburg RJ, Verwiel ET, Smeitink JA, Willems PH, Koopman WJ. Trolox-sensitive reactive oxygen species regulate mitochondrial morphology, oxidative phosphorylation and cytosolic calcium handling in healthy cells. Antioxid Redox Signal 2012; 17: 1657-69.
[39] Grav HJ, Tronstad KJ, Gudbrandsen OA, Berge K, Fladmark KE, Martinsen TC, Waldum H, Wergedahl H, Berge RK. Changed energy state and increased mitochondrial beta-oxidation rate in liver of rats associated with lowered proton electrochemical potential and stimulated uncoupling protein 2 (UCP-2) expression: evidence for peroxisome proliferator-activated receptor-alpha independent induction of UCP-2 expression. J Biol Chem 2003; 278: 30525-33.
[40] Hagland HR, Nilsson LI, Burri L, Nikolaisen J, Berge RK, Tronstad KJ. Induction of mitochondrial biogenesis and respiration is associated with mTOR regulation in hepatocytes

of rats treated with the pan-PPAR activator tetradecylthioacetic acid (TTA). Biochem Biophys Res Commun 2013; 430: 573-8.
[41] Kryvi H, Aarsland A, Berge RK. Morphologic effects of sulfur-substituted fatty acids on rat hepatocytes with special reference to proliferation of peroxisomes and mitochondria. J Struct Biol 1990; 103: 257-65.
[42] Scarpulla RC. Transcriptional paradigms in mammalian mitochondrial biogenesis and function. Physiol Rev 2008; 88: 611-38.
[43] Wellen KE, Thompson CB. Cellular Metabolic Stress: Considering How Cells Respond to Nutrient Excess. Mol Cell 2010; 40: 323-332.
[44] Lunt SY, Vander Heiden MG. Aerobic glycolysis: meeting the metabolic requirements of cell proliferation. Annu Rev Cell Dev Biol 2011; 27: 441-64.
[45] Benard G, Faustin B, Passerieux E, Galinier A, Rocher C, Bellance N, Delage JP, Casteilla L, Letellier T, Rossignol R. Physiological diversity of mitochondrial oxidative phosphorylation. Am J Physiol Cell Physiol 2006; 291: C1172-C1182.
[46] Ventura-Clapier R, Garnier A, Veksler V. Transcriptional control of mitochondrial biogenesis: the central role of PGC-1alpha. Cardiovasc Res 2008; 79: 208-17.
[47] Scarpulla RC. Transcriptional activators and coactivators in the nuclear control of mitochondrial function in mammalian cells. Gene 2002; 286: 81-9.
[48] Chow LS, Greenlund LJ, Asmann YW, Short KR, McCrady SK, Levine JA, Nair KS. Impact of endurance training on murine spontaneous activity, muscle mitochondrial DNA abundance, gene transcripts, and function. J Appl Physiol 2007; 102: 1078-89.
[49] Civitarese AE, Carling S, Heilbronn LK, Hulver MH, Ukropcova B, Deutsch WA, Smith SR, Ravussin E. Calorie restriction increases muscle mitochondrial biogenesis in healthy humans. PLoS medicine 2007; 4: e76.
[50] Ricquier D, Bouillaud F. Mitochondrial uncoupling proteins: from mitochondria to the regulation of energy balance. J Physiol 2000; 529 Pt 1: 3-10.
[51] Cannon B, Nedergaard J. Brown adipose tissue: function and physiological significance. Physiol Rev 2004; 84: 277-359.
[52] Tata JR, Ernster L, Lindberg O, Arrhenius E, Pedersen S, Hedman R. The action of thyroid hormones at the cell level. Biochem J 1963; 86: 408-28.
[53] Michaels GS, Hauswirth WW, Laipis PJ. Mitochondrial DNA copy number in bovine oocytes and somatic cells. Dev Biol 1982; 94: 246-51.
[54] Piko L, Taylor KD. Amounts of mitochondrial DNA and abundance of some mitochondrial gene transcripts in early mouse embryos. Dev Biol 1987; 123: 364-74.
[55] Heerdt BG, Augenlicht LH. Changes in the number of mitochondrial genomes during human development. Exp Cell Res 1990; 186: 54-9.
[56] Folmes CD, Dzeja PP, Nelson TJ, Terzic A. Metabolic plasticity in stem cell homeostasis and differentiation. Cell Stem Cell 2012; 11: 596-606.
[57] Huttemann M, Lee I, Samavati L, Yu H, Doan JW. Regulation of mitochondrial oxidative phosphorylation through cell signaling. Biochim Biophys Acta 2007; 1773: 1701-20.
[58] Hock MB, Kralli A. Transcriptional control of mitochondrial biogenesis and function. Annu Rev Physiol 2009; 71: 177-203.
[59] Arnold S. Cytochrome c oxidase and its role in neurodegeneration and neuroprotection. Adv Exp Med Biol 2012; 748: 305-39.
[60] DiMauro S, Schon EA. Mitochondrial respiratory-chain diseases. N Engl J Med 2003; 348: 2656-68.
[61] Becker T, Bottinger L, Pfanner N. Mitochondrial protein import: from transport pathways to an integrated network. Trends Biochem Sci 2012; 37: 85-91.
[62] Diaz F, Moraes CT. Mitochondrial biogenesis and turnover. Cell Calcium 2008; 44: 24-35.
[63] Elstner M, Turnbull DM. Transcriptome analysis in mitochondrial disorders. Brain Res Bull 2012; 88: 285-93.
[64] Ryan MT, Hoogenraad NJ. Mitochondrial-nuclear communications. Annu Rev Biochem 2007; 76: 701-22.

[65] Scarpulla RC. Metabolic control of mitochondrial biogenesis through the PGC-1 family regulatory network. Biochim Biophys Acta 2011; 1813: 1269-78.
[66] Wu Z, Puigserver P, Andersson U, Zhang C, Adelmant G, Mootha V, Troy A, Cinti S, Lowell B, Scarpulla RC, Spiegelman BM. Mechanisms controlling mitochondrial biogenesis and respiration through the thermogenic coactivator PGC-1. Cell 1999; 98: 115-24.
[67] Puigserver P, Wu Z, Park CW, Graves R, Wright M, Spiegelman BM. A cold-inducible coactivator of nuclear receptors linked to adaptive thermogenesis. Cell 1998; 92: 829-39.
[68] Garnier A, Fortin D, Deloménie C, Momken I, Veksler V, Ventura-Clapier R. Depressed mitochondrial transcription factors and oxidative capacity in rat failing cardiac and skeletal muscles. J Physiol 2003; 551: 491-501.
[69] Schreiber SN, Emter R, Hock MB, Knutti D, Cardenas J, Podvinec M, Oakeley EJ, Kralli A. The estrogen-related receptor alpha (ERRalpha) functions in PPARgamma coactivator 1alpha (PGC-1alpha)-induced mitochondrial biogenesis. Proc Natl Acad Sci USA 2004; 101: 6472-7.
[70] Michael LF, Wu Z, Cheatham RB, Puigserver P, Adelmant G, Lehman JJ, Kelly DP, Spiegelman BM. Restoration of insulin-sensitive glucose transporter (GLUT4) gene expression in muscle cells by the transcriptional coactivator PGC-1. Proc Natl Acad Sci USA 2001; 98: 3820-5.
[71] Baar K, Song Z, Semenkovich CF, Jones TE, Han D-H, Nolte LA, Ojuka EO, Chen MAY, Holloszy JO. Skeletal muscle overexpression of nuclear respiratory factor 1 increases glucose transport capacity. FASEB J 2003; 17: 1666-1673.
[72] Evans MJ, Scarpulla RC. NRF-1: a trans-activator of nuclear-encoded respiratory genes in animal cells. Genes Dev 1990; 4: 1023-34.
[73] Virbasius CA, Virbasius JV, Scarpulla RC. NRF-1, an activator involved in nuclear-mitochondrial interactions, utilizes a new DNA-binding domain conserved in a family of developmental regulators. Genes Dev 1993; 7: 2431-45.
[74] Gugneja S, Scarpulla RC. Serine phosphorylation within a concise amino-terminal domain in nuclear respiratory factor 1 enhances DNA binding. J Biol Chem 1997; 272: 18732-9.
[75] Herzig RP, Scacco S, Scarpulla RC. Sequential serum-dependent activation of CREB and NRF-1 leads to enhanced mitochondrial respiration through the induction of cytochrome c. J Biol Chem 2000; 275: 13134-41.
[76] FitzGerald PC, Shlyakhtenko A, Mir AA, Vinson C. Clustering of DNA sequences in human promoters. Genome Res 2004; 14: 1562-74.
[77] Cam H, Balciunaite E, Blais A, Spektor A, Scarpulla RC, Young R, Kluger Y, Dynlacht BD. A common set of gene regulatory networks links metabolism and growth inhibition. Mol Cell 2004; 16: 399-411.
[78] Kelly DP, Scarpulla RC. Transcriptional regulatory circuits controlling mitochondrial biogenesis and function. Genes Dev 2004; 18: 357-68.
[79] Braidotti G, Borthwick IA, May BK. Identification of regulatory sequences in the gene for 5-aminolevulinate synthase from rat. J Biol Chem 1993; 268: 1109-17.
[80] Blesa JR, Prieto-Ruiz JA, Hernandez JM, Hernandez-Yago J. NRF-2 transcription factor is required for human TOMM20 gene expression. Gene 2007; 391: 198-208.
[81] Blesa JR, Prieto-Ruiz JA, Abraham BA, Harrison BL, Hegde AA, Hernandez-Yago J. NRF-1 is the major transcription factor regulating the expression of the human TOMM34 gene. Biochem Cell Biol 2008; 86: 46-56.
[82] Virbasius JV, Scarpulla RC. Activation of the human mitochondrial transcription factor A gene by nuclear respiratory factors: a potential regulatory link between nuclear and mitochondrial gene expression in organelle biogenesis. Proc Natl Acad Sci USA 1994; 91: 1309-13.
[83] Gleyzer N, Vercauteren K, Scarpulla RC. Control of mitochondrial transcription specificity factors (TFB1M and TFB2M) by nuclear respiratory factors (NRF-1 and NRF-2) and PGC-1 family coactivators. Mol Cell Biol 2005; 25: 1354-66.
[84] Scarpulla RC. Nuclear control of respiratory chain expression by nuclear respiratory factors and PGC-1-related coactivator. Ann N Y Acad Sci 2008; 1147: 321-34.

[85] Patti ME, Butte AJ, Crunkhorn S, Cusi K, Berria R, Kashyap S, Miyazaki Y, Kohane I, Costello M, Saccone R, Landaker EJ, Goldfine AB, Mun E, DeFronzo R, Finlayson J, Kahn CR, Mandarino LJ. Coordinated reduction of genes of oxidative metabolism in humans with insulin resistance and diabetes: Potential role of PGC1 and NRF1. Proc Natl Acad Sci USA 2003; 100: 8466-71.
[86] Murakami T, Shimomura Y, Yoshimura A, Sokabe M, Fujitsuka N. Induction of nuclear respiratory factor-1 expression by an acute bout of exercise in rat muscle. Biochim Biophys Acta 1998; 1381: 113-22.
[87] Miranda S, Foncea R, Guerrero J, Leighton F. Oxidative stress and upregulation of mitochondrial biogenesis genes in mitochondrial DNA-depleted HeLa cells. Biochem Biophys Res Commun 1999; 258: 44-9.
[88] Suliman HB, Carraway MS, Welty-Wolf KE, Whorton AR, Piantadosi CA. Lipopolysaccharide stimulates mitochondrial biogenesis via activation of nuclear respiratory factor-1. J Biol Chem 2003; 278: 41510-8.
[89] Bergeron R, Ren JM, Cadman KS, Moore IK, Perret P, Pypaert M, Young LH, Semenkovich CF, Shulman GI. Chronic activation of AMP kinase results in NRF-1 activation and mitochondrial biogenesis. Am J Physiol Endocrinol Metab 2001; 281: E1340-6.
[90] Reznick RM, Shulman GI. The role of AMP-activated protein kinase in mitochondrial biogenesis. J Physiol 2006; 574: 33-9.
[91] Hardie DG. AMP-activated protein kinase: an energy sensor that regulates all aspects of cell function. Genes Dev 2011; 25: 1895-908.
[92] Terada S, Goto M, Kato M, Kawanaka K, Shimokawa T, Tabata I. Effects of low-intensity prolonged exercise on PGC-1 mRNA expression in rat epitrochlearis muscle. Biochem Biophys Res Commun 2002; 296: 350-4.
[93] Zong H, Ren JM, Young LH, Pypaert M, Mu J, Birnbaum MJ, Shulman GI. AMP kinase is required for mitochondrial biogenesis in skeletal muscle in response to chronic energy deprivation. Proc Natl Acad Sci USA 2002; 99: 15983-7.
[94] Scarpulla RC. Nuclear activators and coactivators in mammalian mitochondrial biogenesis. Biochim Biophys Acta 2002; 1576: 1-14.
[95] Narkar VA, Downes M, Yu RT, Embler E, Wang YX, Banayo E, Mihaylova MM, Nelson MC, Zou Y, Juguilon H, Kang H, Shaw RJ, Evans RM. AMPK and PPARdelta agonists are exercise mimetics. Cell 2008; 134: 405-15.
[96] Yu L, Yang SJ. AMP-activated protein kinase mediates activity-dependent regulation of peroxisome proliferator-activated receptor gamma coactivator-1alpha and nuclear respiratory factor 1 expression in rat visual cortical neurons. Neuroscience 2010; 169: 23-38.
[97] Golubitzky A, Dan P, Weissman S, Link G, Wikstrom JD, Saada A. Screening for active small molecules in mitochondrial complex I deficient patient's fibroblasts, reveals AICAR as the most beneficial compound. PloS one 2011; 6: e26883.
[98] Viscomi C, Bottani E, Civiletto G, Cerutti R, Moggio M, Fagiolari G, Schon EA, Lamperti C, Zeviani M. In vivo correction of COX deficiency by activation of the AMPK/PGC-1alpha axis. Cell Metab 2011; 14: 80-90.
[99] Lezza AM, Pesce V, Cormio A, Fracasso F, Vecchiet J, Felzani G, Cantatore P, Gadaleta MN. Increased expression of mitochondrial transcription factor A and nuclear respiratory factor-1 in skeletal muscle from aged human subjects. FEBS Lett 2001; 501: 74-8.
[100] Virbasius JV, Scarpulla RC. Transcriptional activation through ETS domain binding sites in the cytochrome c oxidase subunit IV gene. Mol Cell Biol 1991; 11: 5631-8.
[101] Escher P, Wahli W. Peroxisome proliferator-activated receptors: insight into multiple cellular functions. Mutat Res 2000; 448: 121-38.
[102] Moreno M, Lombardi A, Silvestri E, Senese R, Cioffi F, Goglia F, Lanni A, de Lange P. PPARs: Nuclear Receptors Controlled by, and Controlling, Nutrient Handling through Nuclear and Cytosolic Signaling. PPAR Res 2010; 2010: doi:pii: 435689. 10.1155/2010/435689.
[103] Finck BN. The PPAR regulatory system in cardiac physiology and disease. Cardiovasc Res 2007; 73: 269-77.

[104] Ahmed W, Ziouzenkova O, Brown J, Devchand P, Francis S, Kadakia M, Kanda T, Orasanu G, Sharlach M, Zandbergen F, Plutzky J. PPARs and their metabolic modulation: new mechanisms for transcriptional regulation? J Intern Med 2007; 262: 184-98.
[105] Tachibana K, Yamasaki D, Ishimoto K, Doi T. The Role of PPARs in Cancer. PPAR Res 2008; 2008: doi: 10.1155/2008/102737.
[106] Ravnskjaer K, Frigerio F, Boergesen M, Nielsen T, Maechler P, Mandrup S. PPARδ is a fatty acid sensor that enhances mitochondrial oxidation in insulin-secreting cells and protects against fatty acid-induced dysfunction. J Lipid Res 2010; 51: 1370-1379.
[107] Lehrke M, Lazar MA. The many faces of PPARgamma. Cell 2005; 123: 993-9.
[108] Cartoni R, Leger B, Hock MB, Praz M, Crettenand A, Pich S, Ziltener JL, Luthi F, Deriaz O, Zorzano A, Gobelet C, Kralli A, Russell AP. Mitofusins 1/2 and ERRalpha expression are increased in human skeletal muscle after physical exercise. J Physiol 2005; 567: 349-58.
[109] Giguere V. Transcriptional control of energy homeostasis by the estrogen-related receptors. Endocr Rev 2008; 29: 677-96.
[110] McCoy MK, Cookson MR. Mitochondrial quality control and dynamics in Parkinson's disease. Antioxid Redox Signal 2012; 16: 869-82.
[111] Court FA, Coleman MP. Mitochondria as a central sensor for axonal degenerative stimuli. Trends Neurosci 2012; 35: 364-72.
[112] Youle RJ, van der Bliek AM. Mitochondrial fission, fusion, and stress. Science 2012; 337: 1062-5.
[113] Jeyaraju DV, Sood A, Laforce-Lavoie A, Pellegrini L. Rhomboid proteases in mitochondria and plastids: keeping organelles in shape. Biochim Biophys Acta 2013; 1833: 371-80.
[114] Voos W. Chaperone-protease networks in mitochondrial protein homeostasis. Biochim Biophys Acta 2013; 1833: 388-99.
[115] Jin SM, Lazarou M, Wang C, Kane LA, Narendra DP, Youle RJ. Mitochondrial membrane potential regulates PINK1 import and proteolytic destabilization by PARL. J Cell Biol 2010; 191: 933-42.
[116] Matsuda N, Sato S, Shiba K, Okatsu K, Saisho K, Gautier CA, Sou YS, Saiki S, Kawajiri S, Sato F, Kimura M, Komatsu M, Hattori N, Tanaka K. PINK1 stabilized by mitochondrial depolarization recruits Parkin to damaged mitochondria and activates latent Parkin for mitophagy. J Cell Biol 2010; 189: 211-21.
[117] Meissner C, Lorenz H, Weihofen A, Selkoe DJ, Lemberg MK. The mitochondrial intramembrane protease PARL cleaves human Pink1 to regulate Pink1 trafficking. J Neurochem 2011; 117: 856-67.
[118] Tanaka A, Cleland MM, Xu S, Narendra DP, Suen DF, Karbowski M, Youle RJ. Proteasome and p97 mediate mitophagy and degradation of mitofusins induced by Parkin. J Cell Biol 2010; 191: 1367-80.
[119] Kitada T, Asakawa S, Hattori N, Matsumine H, Yamamura Y, Minoshima S, Yokochi M, Mizuno Y, Shimizu N. Mutations in the parkin gene cause autosomal recessive juvenile parkinsonism. Nature 1998; 392: 605-8.
[120] Valente EM, Abou-Sleiman PM, Caputo V, Muqit MM, Harvey K, Gispert S, Ali Z, Del Turco D, Bentivoglio AR, Healy DG, Albanese A, Nussbaum R, Gonzalez-Maldonado R, Deller T, Salvi S, Cortelli P, Gilks WP, Latchman DS, Harvey RJ, Dallapiccola B, Auburger G, Wood NW. Hereditary early-onset Parkinson's disease caused by mutations in PINK1. Science 2004; 304: 1158-60.
[121] Choubey V, Safiulina D, Vaarmann A, Cagalinec M, Wareski P, Kuum M, Zharkovsky A, Kaasik A. Mutant A53T alpha-synuclein induces neuronal death by increasing mitochondrial autophagy. J Biol Chem 2011; 286: 10814-24.
[122] Nakamura K, Nemani VM, Azarbal F, Skibinski G, Levy JM, Egami K, Munishkina L, Zhang J, Gardner B, Wakabayashi J, Sesaki H, Cheng Y, Finkbeiner S, Nussbaum RL, Masliah E, Edwards RH. Direct membrane association drives mitochondrial fission by the Parkinson disease-associated protein alpha-synuclein. J Biol Chem 2011; 286: 20710-26.
[123] Xie W, Chung KK. Alpha-synuclein impairs normal dynamics of mitochondria in cell and animal models of Parkinson's disease. J Neurochem 2012.

[124] Shin JH, Ko HS, Kang H, Lee Y, Lee YI, Pletinkova O, Troconso JC, Dawson VL, Dawson TM. PARIS (ZNF746) repression of PGC-1alpha contributes to neurodegeneration in Parkinson's disease. Cell 2011; 144: 689-702.
[125] Kubli DA, Gustafsson AB. Mitochondria and mitophagy: the yin and yang of cell death control. Circulation research 2012; 111: 1208-21.
[126] Novak I. Mitophagy: a complex mechanism of mitochondrial removal. Antioxidants & redox signaling 2012; 17: 794-802.
[127] Sun Y, Vashisht AA, Tchieu J, Wohlschlegel JA, Dreier L. Voltage-dependent anion channels (VDACs) recruit Parkin to defective mitochondria to promote mitochondrial autophagy. J Biol Chem 2012; 287: 40652-60.
[128] Kim NC, Tresse E, Kolaitis RM, Molliex A, Thomas RE, Alami NH, Wang B, Joshi A, Smith RB, Ritson GP, Winborn BJ, Moore J, Lee JY, Yao TP, Pallanck L, Kundu M, Taylor JP. VCP Is Essential for Mitochondrial Quality Control by PINK1/Parkin and this Function Is Impaired by VCP Mutations. Neuron 2013; Mar 13 [Epub ahead of print].
[129] Cortese JD. Rat liver GTP-binding proteins mediate changes in mitochondrial membrane potential and organelle fusion. Am J Physiol 1999; 276: C611-20.
[130] Frederick RL, Shaw JM. Moving mitochondria: establishing distribution of an essential organelle. Traffic 2007; 8: 1668-75.
[131] Pucci B, Bertani F, Karpinich NO, Indelicato M, Russo MA, Farber JL, Tafani M. Detailing the role of Bax translocation, cytochrome c release, and perinuclear clustering of the mitochondria in the killing of HeLa cells by TNF. J Cell Physiol 2008; 217: 442-9.
[132] Kornmann B, Currie E, Collins SR, Schuldiner M, Nunnari J, Weissman JS, Walter P. An ER-mitochondria tethering complex revealed by a synthetic biology screen. Science 2009; 325: 477-81.
[133] Frazier AE, Kiu C, Stojanovski D, Hoogenraad NJ, Ryan MT. Mitochondrial morphology and distribution in mammalian cells. Biol Chem 2006; 387: 1551-8.
[134] Bleazard W, McCaffery JM, King EJ, Bale S, Mozdy A, Tieu Q, Nunnari J, Shaw JM. The dynamin-related GTPase Dnm1 regulates mitochondrial fission in yeast. Nat Cell Biol 1999; 1: 298-304.
[135] Frank S, Gaume B, Bergmann-Leitner ES, Leitner WW, Robert EG, Catez F, Smith CL, Youle RJ. The role of dynamin-related protein 1, a mediator of mitochondrial fission, in apoptosis. Dev Cell 2001; 1: 515-25.
[136] Karbowski M, Youle RJ. Dynamics of mitochondrial morphology in healthy cells and during apoptosis. Cell Death Differ 2003; 10: 870-80.
[137] Cipolat S, Martins de Brito O, Dal Zilio B, Scorrano L. OPA1 requires mitofusin 1 to promote mitochondrial fusion. Proc Natl Acad Sci USA 2004; 101: 15927-32.
[138] Malka F, Guillery O, Cifuentes-Diaz C, Guillou E, Belenguer P, Lombes A, Rojo M. Separate fusion of outer and inner mitochondrial membranes. EMBO Rep 2005; 6: 853-9.
[139] Chan DC. Mitochondrial fusion and fission in mammals. Annu Rev Cell Dev Biol 2006; 22: 79-99.
[140] Knott AB, Perkins G, Schwarzenbacher R, Bossy-Wetzel E. Mitochondrial fragmentation in neurodegeneration. Nature reviews. Neuroscience 2008; 9: 505-18.
[141] Otera H, Ishihara N, Mihara K. New insights into the function and regulation of mitochondrial fission. Biochim Biophys Acta 2013; 1833: 1256-68.
[142] Belenguer P, Pellegrini L. The dynamin GTPase OPA1: more than mitochondria? Biochim Biophys Acta 2013; 1833: 176-83.
[143] Elgass K, Pakay J, Ryan MT, Palmer CS. Recent advances into the understanding of mitochondrial fission. Biochim Biophys Acta 2013; 1833: 150-61.
[144] Korobova F, Ramabhadran V, Higgs HN. An actin-dependent step in mitochondrial fission mediated by the ER-associated formin INF2. Science 2013; 339: 464-7.
[145] Loson OC, Song Z, Chen H, Chan DC. Fis1, Mff, MiD49, and MiD51 mediate Drp1 recruitment in mitochondrial fission. Mol Biol Cell 2013; 24: 659-67.
[146] Onoue K, Jofuku A, Ban-Ishihara R, Ishihara T, Maeda M, Koshiba T, Itoh T, Fukuda M, Otera H, Oka T, Takano H, Mizushima N, Mihara K, Ishihara N. Fis1 acts as a mitochondrial

recruitment factor for TBC1D15 that is involved in regulation of mitochondrial morphology. J Cell Sci 2013; 126: 176-85.
[147] Shutt T, Geoffrion M, Milne R, McBride HM. The intracellular redox state is a core determinant of mitochondrial fusion. EMBO Rep 2012; 13: 909-15.
[148] Westermann B. Bioenergetic role of mitochondrial fusion and fission. Biochim Biophys Acta 2012; 1817: 1833-8.
[149] Koopman WJ, Visch HJ, Verkaart S, van den Heuvel LW, Smeitink JA, Willems PH. Mitochondrial network complexity and pathological decrease in complex I activity are tightly correlated in isolated human complex I deficiency. Am J Physiol Cell Physiol 2005; 289: C881-90.
[150] Koopman WJ, Verkaart S, Visch HJ, van Emst-de Vries S, Nijtmans LG, Smeitink JA, Willems PH. Human NADH:ubiquinone oxidoreductase deficiency: radical changes in mitochondrial morphology? Am J Physiol Cell Physiol 2007; 293: C22-9.
[151] Supale S, Li N, Brun T, Maechler P. Mitochondrial dysfunction in pancreatic beta cells. Trends in endocrinology and metabolism: Trends Endocrinol Metab 2012; 23: 477-87
[152] Van Laar VS, Berman SB. The interplay of neuronal mitochondrial dynamics and bioenergetics: implications for Parkinson's disease. Neurobiol Dis 2013; 51: 43-55.
[153] Romanello V, Sandri M. Mitochondrial biogenesis and fragmentation as regulators of protein degradation in striated muscles. J Mol Cell Cardiol 2013; 55: 64-72.
[154] Picard M, Shirihai OS, Gentil BJ, Burelle Y. Mitochondrial morphology transitions and functions: implications for retrograde signaling? Am J Physiol Regul Integr Comp Physiol 2013; 304: R393-406.
[155] Zhan M, Brooks C, Liu F, Sun L, Dong Z. Mitochondrial dynamics: regulatory mechanisms and emerging role in renal pathophysiology. Kidney Int 2013; 83: 568-81.
[156] Egner A, Jakobs S, Hell SW. Fast 100-nm resolution three-dimensional microscope reveals structural plasticity of mitochondria in live yeast. Proc Natl Acad Sci USA 2002; 99: 3370-5.
[157] Liesa M, Borda-d'Agua B, Medina-Gomez G, Lelliott CJ, Paz JC, Rojo M, Palacin M, Vidal-Puig A, Zorzano A. Mitochondrial fusion is increased by the nuclear coactivator PGC-1beta. PloS one 2008; 3: e3613.
[158] Pich S, Bach D, Briones P, Liesa M, Camps M, Testar X, Palacin M, Zorzano A. The Charcot-Marie-Tooth type 2A gene product, Mfn2, up-regulates fuel oxidation through expression of OXPHOS system. Hum Mol Genet 2005; 14: 1405-15.
[159] Cereghetti GM, Scorrano L. The many shapes of mitochondrial death. Oncogene 2006; 25: 4717-24.
[160] Benard G, Bellance N, James D, Parrone P, Fernandez H, Letellier T, Rossignol R. Mitochondrial bioenergetics and structural network organization. J Cell Sci 2007; 120: 838-48.
[161] Bindoff LA, Desnuelle C, Birch-Machin MA, Pellissier JF, Serratrice G, Dravet C, Bureau M, Howell N, Turnbull DM. Multiple defects of the mitochondrial respiratory chain in a mitochondrial encephalopathy (MERRF): a clinical, biochemical and molecular study. J Neurol Sci 1991; 102: 17-24.
[162] Willems PH, Smeitink JA, Koopman WJ. Mitochondrial dynamics in human NADH:ubiquinone oxidoreductase deficiency. Int J Biochem Cell Biol 2009; 41: 1773-82.
[163] Koopman WJ, Hink MA, Verkaart S, Visch HJ, Smeitink JA, Willems PH. Partial complex I inhibition decreases mitochondrial motility and increases matrix protein diffusion as revealed by fluorescence correlation spectroscopy. Biochim Biophys Acta 2007; 1767: 940-7.
[164] Takanashi H, Ohnishi T, Mogi M, Okamoto T, Arimura S, Tsutsumi N. Studies of mitochondrial morphology and DNA amount in the rice egg cell. Curr Genet 2010; 56: 33-41.
[165] Barbieri E, Battistelli M, Casadei L, Vallorani L, Piccoli G, Guescini M, Gioacchini AM, Polidori E, Zeppa S, Ceccaroli P, Stocchi L, Stocchi V, Falcieri E. Morphofunctional and Biochemical Approaches for Studying Mitochondrial Changes during Myoblasts Differentiation. J Aging Res 2011; 2011: doi: 10.4061/2011/845379.

[166] Froyland L, Helland K, Totland GK, Kryvi H, Berge RK. A hypolipidemic peroxisome proliferating fatty acid induces polydispersity of rat liver mitochondria. Biol Cell 1996; 87: 105-12.
[167] Santoro C, Cosmas A, Forman D, Morghan A, Bairos L, Levesque S, Roubenoff R, Hennessey J, Lamont L, Manfredi T. Exercise training alters skeletal muscle mitochondrial morphometry in heart failure patients. J Cardiovasc Risk 2002; 9: 377-81.
[168] Cury DP, Dias FJ, Sosthenes MC, Dos Santos Haemmerle CA, Ogawa K, Da Silva MC, Mardegan Issa JP, Iyomasa MM, Watanabe IS. Morphometric, quantitative, and three-dimensional analysis of the heart muscle fibers of old rats: Transmission electron microscopy and high-resolution scanning electron microscopy methods. Microsc Res Tech 2012.
[169] Weibel ER. Stereological principles for morphometry in electron microscopic cytology. Int Rev Cytol 1969; 26: 235-302.
[170] Frey TG, Mannella CA. The internal structure of mitochondria. Trends Biochem Sci 2000; 25: 319-24.
[171] Frey TG, Sun MG. Correlated light and electron microscopy illuminates the role of mitochondrial inner membrane remodeling during apoptosis. Biochim Biophys Acta 2008; 1777: 847-52.
[172] Perkins G, Bossy-Wetzel E, Ellisman MH. New insights into mitochondrial structure during cell death. Exp Neurol 2009; 218: 183-92.
[173] Hoppel CL, Tandler B, Fujioka H, Riva A. Dynamic organization of mitochondria in human heart and in myocardial disease. Int J Biochem Cell Biol 2009; 41: 1949-56.
[174] Koning RI, Koster AJ. Cryo-electron tomography in biology and medicine. Ann Anat 2009; 191: 427-45.
[175] Arismendi-Morillo G. Electron microscopy morphology of the mitochondrial network in human cancer. Int J Biochem Cell Biol 2009; 41: 2062-8.
[176] Dudkina NV, Kouril R, Bultema JB, Boekema EJ. Imaging of organelles by electron microscopy reveals protein-protein interactions in mitochondria and chloroplasts. FEBS Lett 2010; 584: 2510-5.
[177] Arismendi-Morillo G. Electron microscopy morphology of the mitochondrial network in gliomas and their vascular microenvironment. Biochim Biophys Acta 2011; 1807: 602-8.
[178] Ding WX, Li M, Biazik JM, Morgan DG, Guo F, Ni HM, Goheen M, Eskelinen EL, Yin XM. Electron microscopic anal ysis of a spherical mitochondrial structure. J Biol Chem 2012.
[179] Giuly RJ, Martone ME, Ellisman MH. Method: automatic segmentation of mitochondria utilizing patch classification, contour pair classification, and automatically seeded level sets. BMC Bioinformatics 2012; 13: 29.
[180] Mumcuoglu EU, Hassanpour R, Tasel SF, Perkins G, Martone ME, Gurcan MN. Computerized detection and segmentation of mitochondria on electron microscope images. J Microsc 2012; 246: 248-65.
[181] Kuznetsov AV, Veksler V, Gellerich FN, Saks V, Margreiter R, Kunz WS. Analysis of mitochondrial function in situ in permeabilized muscle fibers, tissues and cells. Nat Protoc 2008; 3: 965-76.
[182] Pesta D, Gnaiger E. High-resolution respirometry: OXPHOS protocols for human cells and permeabilized fibers from small biopsies of human muscle. Methods Mol Biol 2012; 810: 25-58.
[183] Ruiz M, Courilleau D, Jullian JC, Fortin D, Ventura-Clapier R, Blondeau JP, Garnier A. A Cardiac-Specific Robotized Cellular Assay Identified Families of Human Ligands as Inducers of PGC-1alpha Expression and Mitochondrial Biogenesis. PloS one 2012; 7: e46753.
[184] Smolkova K, Bellance N, Scandurra F, Genot E, Gnaiger E, Plecita-Hlavata L, Jezek P, Rossignol R. Mitochondrial bioenergetic adaptations of breast cancer cells to aglycemia and hypoxia. J Bioenerg Biomembr 2010; 42: 55-67.
[185] Erikstein BS, Hagland HR, Nikolaisen J, Kulawiec M, Singh KK, Gjertsen BT, Tronstad KJ. Cellular stress induced by resazurin leads to autophagy and cell death via production of reactive oxygen species and mitochondrial impairment. J Cell Biochem 2010; 111: 574-84.

[186] Chance B, Williams GR. The respiratory chain and oxidative phosphorylation. Adv Enzymol Relat Subj Biochem 1956; 17: 65-134.
[187] Williams GR. Dynamic Aspects of the Tricarboxylic Acid Cycle in Isolated Mitochondria. Can J Biochem Physiol 1965; 43: 603-15.
[188] Nedergaard J, Cannon B. Overview--preparation and properties of mitochondria from different sources. Methods Enzymol 1979; 55: 3-28.
[189] Frezza C, Cipolat S, Scorrano L. Organelle isolation: functional mitochondria from mouse liver, muscle and cultured fibroblasts. Nat Protoc 2007; 2: 287-95.
[190] Picard M, Taivassalo T, Ritchie D, Wright KJ, Thomas MM, Romestaing C, Hepple RT. Mitochondrial structure and function are disrupted by standard isolation methods. PloS one 2011; 6: e18317.
[191] Saks VA, Veksler VI, Kuznetsov AV, Kay L, Sikk P, Tiivel T, Tranqui L, Olivares J, Winkler K, Wiedemann F, Kunz WS. Permeabilized cell and skinned fiber techniques in studies of mitochondrial function in vivo. Mol Cell Biochem 1998; 184: 81-100.
[192] Picard M, Taivassalo T, Gouspillou G, Hepple RT. Mitochondria: isolation, structure and function. J Physiol 2011; 589: 4413-21.
[193] Spinazzi M, Casarin A, Pertegato V, Salviati L, Angelini C. Assessment of mitochondrial respiratory chain enzymatic activities on tissues and cultured cells. Nat Protoc 2012; 7: 1235-46.
[194] Valsecchi F, Koopman WJ, Manjeri GR, Rodenburg RJ, Smeitink JA, Willems PH. Complex I disorders: causes, mechanisms, and development of treatment strategies at the cellular level. Dev Disabil Res Rev 2010; 16: 175-82.
[195] Niederstatter H, Kochl S, Grubwieser P, Pavlic M, Steinlechner M, Parson W. A modular real-time PCR concept for determining the quantity and quality of human nuclear and mitochondrial DNA. Forensic Sci Int Genet 2007; 1: 29-34.
[196] Duran HE, Simsek-Duran F, Oehninger SC, Jones HW, Jr., Castora FJ. The association of reproductive senescence with mitochondrial quantity, function, and DNA integrity in human oocytes at different stages of maturation. Fertil Steril 2011; 96: 384-8.
[197] Cayci T, Kurt B, Akgul EO, Kurt YG. Quantification of mitochondrial abundance. Fertil Steril 2012; 97: e18.
[198] Malik AN, Czajka A. Is mitochondrial DNA content a potential biomarker of mitochondrial dysfunction? Mitochondrion 2012; Oct 22 [Epub ahead of print].
[199] Trifunovic A, Hansson A, Wredenberg A, Rovio AT, Dufour E, Khvorostov I, Spelbrink JN, Wibom R, Jacobs HT, Larsson NG. Somatic mtDNA mutations cause aging phenotypes without affecting reactive oxygen species production. Proc Natl Acad Sci USA 2005; 102: 17993-8.
[200] Hiona A, Sanz A, Kujoth GC, Pamplona R, Seo AY, Hofer T, Someya S, Miyakawa T, Nakayama C, Samhan-Arias AK, Servais S, Barger JL, Portero-Otin M, Tanokura M, Prolla TA, Leeuwenburgh C. Mitochondrial DNA mutations induce mitochondrial dysfunction, apoptosis and sarcopenia in skeletal muscle of mitochondrial DNA mutator mice. PloS one 2010; 5: e11468.
[201] Kaneko S, Iida RH, Suga T, Fukui T, Morito M, Yamane A. Changes in triacylglycerol-accumulated fiber type, fiber type composition, and biogenesis in the mitochondria of the soleus muscle in obese rats. Anat Rec (Hoboken) 2011; 294: 1904-12.
[202] Crugnola V, Lamperti C, Lucchini V, Ronchi D, Peverelli L, Prelle A, Sciacco M, Bordoni A, Fassone E, Fortunato F, Corti S, Silani V, Bresolin N, Di Mauro S, Comi GP, Moggio M. Mitochondrial respiratory chain dysfunction in muscle from patients with amyotrophic lateral sclerosis. Arch Neurol 2010; 67: 849-54.
[203] Mensink M, Hesselink MK, Russell AP, Schaart G, Sels JP, Schrauwen P. Improved skeletal muscle oxidative enzyme activity and restoration of PGC-1 alpha and PPAR beta/delta gene expression upon rosiglitazone treatment in obese patients with type 2 diabetes mellitus. Int J Obes (Lond) 2007; 31: 1302-10.

[204] Wagatsuma A, Kotake N, Mabuchi K, Yamada S. Expression of nuclear-encoded genes involved in mitochondrial biogenesis and dynamics in experimentally denervated muscle. J Physiol Biochem 2011; 67: 359-70.
[205] Ernster L, Schatz G. Mitochondria: a historical review. J Cell Biol 1981; 91: 227s-255s.
[206] Hell SW. Microscopy and its focal switch. Nat Methods 2009; 6: 24-32.
[207] Patterson G, Davidson M, Manley S, Lippincott-Schwartz J. Superresolution imaging using single-molecule localization. Annu Rev Phys Chem 2010; 61: 345-67.
[208] Brown TA, Tkachuk AN, Shtengel G, Kopek BG, Bogenhagen DF, Hess HF, Clayton DA. Superresolution fluorescence imaging of mitochondrial nucleoids reveals their spatial range, limits, and membrane interaction. Mol Cell Biol 2011; 31: 4994-5010.
[209] Kukat C, Wurm CA, Spahr H, Falkenberg M, Larsson NG, Jakobs S. Super-resolution microscopy reveals that mammalian mitochondrial nucleoids have a uniform size and frequently contain a single copy of mtDNA. Proc Natl Acad Sci USA 2011; 108: 13534-9.
[210] Appelhans T, Richter CP, Wilkens V, Hess ST, Piehler J, Busch KB. Nanoscale organization of mitochondrial microcompartments revealed by combining tracking and localization microscopy. Nano Lett 2012; 12: 610-6.
[211] Tonnesen J, Nagerl UV. Superresolution imaging for neuroscience. Exp Neurol 2013; 242: 33-40.
[212] Coltharp C, Xiao J. Superresolution microscopy for microbiology. Cell Microbiol 2012; 14: 1808-18.
[213] Shao L, Kner P, Rego EH, Gustafsson MG. Super-resolution 3D microscopy of live whole cells using structured illumination. Nat Methods 2011; 8: 1044-6.
[214] Forkink M, Smeitink JA, Brock R, Willems PH, Koopman WJ. Detection and manipulation of mitochondrial reactive oxygen species in mammalian cells. Biochim Biophys Acta 2010; 1797: 1034-44.
[215] Nooteboom M, Forkink M, Willems PHGM, Koopman WJH. In Neuromethods 70: Visualization techniques, from immunohistochemistry to Magnetic Resonance Imaging, E. Badoer, ed.; Humana Press, 2012.
[216] Dieteren CE, Gielen SC, Nijtmans LG, Smeitink JA, Swarts HG, Brock R, Willems PH, Koopman WJ. Solute diffusion is hindered in the mitochondrial matrix. Proc Natl Acad Sci USA 2011; 108: 8657-62.
[217] Dieteren CE, Koopman WJ, Swarts HG, Peters JG, Maczuga P, van Gemst JJ, Masereeuw R, Smeitink JA, Nijtmans LG, Willems PH. Subunit-specific incorporation efficiency and kinetics in mitochondrial complex I homeostasis. J Biol Chem 2012; 287: 41851-60.
[218] Vogel RO, Janssen RJ, van den Brand MA, Dieteren CE, Verkaart S, Koopman WJ, Willems PH, Pluk W, van den Heuvel LP, Smeitink JA, Nijtmans LG. Cytosolic signaling protein Ecsit also localizes to mitochondria where it interacts with chaperone NDUFAF1 and functions in complex I assembly. Genes Dev 2007; 21: 615-24.
[219] Koopman WJ, Distelmaier F, Esseling JJ, Smeitink JA, Willems PH. Computer-assisted live cell analysis of mitochondrial membrane potential, morphology and calcium handling. Methods 2008; 46: 304-11.
[220] Distelmaier F, Koopman WJ, Testa ER, de Jong AS, Swarts HG, Mayatepek E, Smeitink JA, Willems PH. Life cell quantification of mitochondrial membrane potential at the single organelle level. Cytometry A 2008; 73: 129-38.
[221] Duchen MR, Surin A, Jacobson J. Imaging mitochondrial function in intact cells. Methods Enzymol 2003; 361: 353-89.
[222] Koopman WJ, Visch HJ, Smeitink JA, Willems PH. Simultaneous quantitative measurement and automated analysis of mitochondrial morphology, mass, potential, and motility in living human skin fibroblasts. Cytometry A 2006; 69: 1-12.
[223] Davidson SM, Yellon D, Duchen MR. Assessing mitochondrial potential, calcium, and redox state in isolated mammalian cells using confocal microscopy. Methods Mol Biol 2007; 372: 421-30.

[224] Campanella M, Seraphim A, Abeti R, Casswell E, Echave P, Duchen MR. IF1, the endogenous regulator of the F(1)F(o)-ATPsynthase, defines mitochondrial volume fraction in HeLa cells by regulating autophagy. Biochim Biophys Acta 2009; 1787: 393-401.
[225] Mortiboys H, Thomas KJ, Koopman WJ, Klaffke S, Abou-Sleiman P, Olpin S, Wood NW, Willems PH, Smeitink JA, Cookson MR, Bandmann O. Mitochondrial function and morphology are impaired in parkin-mutant fibroblasts. Ann Neurol 2008; 64: 555-65.
[226] Komen JC, Distelmaier F, Koopman WJ, Wanders RJ, Smeitink J, Willems PH. Phytanic acid impairs mitochondrial respiration through protonophoric action. Cell Mol Life Sci 2007; 64: 3271-81.
[227] Jonckheere AI, Huigsloot M, Lammens M, Jansen J, van den Heuvel LP, Spiekerkoetter U, von Kleist-Retzow JC, Forkink M, Koopman WJ, Szklarczyk R, Huynen MA, Fransen JA, Smeitink JA, Rodenburg RJ. Restoration of complex V deficiency caused by a novel deletion in the human TMEM70 gene normalizes mitochondrial morphology. Mitochondrion 2011; 11: 954-63.
[228] Willems P, Wanschers BF, Esseling J, Szklarczyk R, Kudla U, Duarte I, Forkink M, Nooteboom M, Swarts H, Gloerich J, Nijtmans L, Koopman W, Huynen MA. BOLA1 is an aerobic protein that prevents mitochondrial morphology changes induced by glutathione depletion. Antioxid Redox Signal 2013; 18: 129-38.
[229] Koopman WJ, Distelmaier F, Hink MA, Verkaart S, Wijers M, Fransen J, Smeitink JA, Willems PH. Inherited complex I deficiency is associated with faster protein diffusion in the matrix of moving mitochondria. Am J Physiol Cell Physiol 2008; 294: C1124-32.
[230] Grunewald A, Voges L, Rakovic A, Kasten M, Vandebona H, Hemmelmann C, Lohmann K, Orolicki S, Ramirez A, Schapira AH, Pramstaller PP, Sue CM, Klein C. Mutant Parkin impairs mitochondrial function and morphology in human fibroblasts. PloS one 2010; 5: e12962.
[231] Rakovic A, Grunewald A, Kottwitz J, Bruggemann N, Pramstaller PP, Lohmann K, Klein C. Mutations in PINK1 and Parkin impair ubiquitination of Mitofusins in human fibroblasts. PloS one 2011; 6: e16746.
[232] Coussee E, De Smet P, Bogaert E, Elens I, Van Damme P, Willems P, Koopman W, Van Den Bosch L, Callewaert G. G37R SOD1 mutant alters mitochondrial complex I activity, Ca(2+) uptake and ATP production. Cell calcium 2011; 49: 217-25.
[233] Eisenberg I, Novershtern N, Itzhaki Z, Becker-Cohen M, Sadeh M, Willems PH, Friedman N, Koopman WJ, Mitrani-Rosenbaum S. Mitochondrial processes are impaired in hereditary inclusion body myopathy. Hum Mol Genet 2008; 17: 3663-74.
[234] Wang X, Yan MH, Fujioka H, Liu J, Wilson-Delfosse A, Chen SG, Perry G, Casadesus G, Zhu X. LRRK2 regulates mitochondrial dynamics and function through direct interaction with DLP1. Hum Mol Genet 2012; 21: 1931-44.
[235] Wang X, Su B, Liu W, He X, Gao Y, Castellani RJ, Perry G, Smith MA, Zhu X. DLP1-dependent mitochondrial fragmentation mediates 1-methyl-4-phenylpyridinium toxicity in neurons: implications for Parkinson's disease. Aging Cell 2011; 10: 807-23.
[236] Heeman B, Van den Haute C, Aelvoet SA, Valsecchi F, Rodenburg RJ, Reumers V, Debyser Z, Callewaert G, Koopman WJ, Willems PH, Baekelandt V. Depletion of PINK1 affects mitochondrial metabolism, calcium homeostasis and energy maintenance. J Cell Sci 2011; 124: 1115-25.
[237] Matthews GD, Gur N, Koopman WJ, Pines O, Vardimon L. Weak mitochondrial targeting sequence determines tissue-specific subcellular localization of glutamine synthetase in liver and brain cells. J Cell Sci 2010; 123: 351-9.
[238] Hoffmann M, Bellance N, Rossignol R, Koopman WJ, Willems PH, Mayatepek E, Bossinger O, Distelmaier F. C. elegans ATAD-3 is essential for mitochondrial activity and development. PloS one 2009; 4: e7644.
[239] Wang X, Petrie TG, Liu Y, Liu J, Fujioka H, Zhu X. Parkinson's disease-associated DJ-1 mutations impair mitochondrial dynamics and cause mitochondrial dysfunction. J Neurochem 2012; 121: 830-9.

[240] De Vos KJ, Allan VJ, Grierson AJ, Sheetz MP. Mitochondrial function and actin regulate dynamin-related protein 1-dependent mitochondrial fission. Curr Biol 2005; 15: 678-83.
[241] De Vos KJ, Sheetz MP. Visualization and quantification of mitochondrial dynamics in living animal cells. Methods Cell Biol 2007; 80: 627-82.
[242] Yu T, Robotham JL, Yoon Y. Increased production of reactive oxygen species in hyperglycemic conditions requires dynamic change of mitochondrial morphology. Proc Natl Acad Sci USA 2006; 103: 2653-8.
[243] Yu T, Sheu SS, Robotham JL, Yoon Y. Mitochondrial fission mediates high glucose-induced cell death through elevated production of reactive oxygen species. Cardiovasc Res 2008; 79: 341-51.
[244] Yu T, Jhun BS, Yoon Y. High-glucose stimulation increases reactive oxygen species production through the calcium and mitogen-activated protein kinase-mediated activation of mitochondrial fission. Antioxid Redox Signal 2011; 14: 425-37.
[245] Cunniff B, Benson K, Stumpff J, Newick K, Held P, Taatjes D, Joseph J, Kalyanaraman B, Heintz NH. Mitochondrial-targeted nitroxides disrupt mitochondrial architecture and inhibit expression of peridoxin 3 and FOXM1 in malignant mesothelioma cells. J Cell Physiol 2013; 228: 835-45.
[246] Lihavainen E, Makela J, Spelbrink JN, Ribeiro AS. Mytoe: automatic analysis of mitochondrial dynamics. Bioinformatics 2012; 28: 1050-1.
[247] Chevrollier A, Cassereau J, Ferre M, Alban J, Desquiret-Dumas V, Gueguen N, Amati-Bonneau P, Procaccio V, Bonneau D, Reynier P. Standardized mitochondrial analysis gives new insights into mitochondrial dynamics and OPA1 function. Int J Biochem Cell Biol 2012; 44: 980-8.
[248] Giedt RJ, Yang C, Zweier JL, Matzavinos A, Alevriadou BR. Mitochondrial fission in endothelial cells after simulated ischemia/reperfusion: role of nitric oxide and reactive oxygen species. Free Radic Biol Med 2012; 52: 348-56.
[249] Peng JY, Lin CC, Chen YJ, Kao LS, Liu YC, Chou CC, Huang YH, Chang FR, Wu YC, Tsai YS, Hsu CN. Automatic morphological subtyping reveals new roles of caspases in mitochondrial dynamics. PLoS Comput Biol 2011; 7: e1002212.
[250] Liu X, Feng L, Yan M, Xu K, Yu Y, Zheng X. Changes in mitochondrial dynamics during amyloid beta-induced PC12 cell apoptosis. Mol Cell Biochem 2010; 344: 277-84.
[251] Dagda RK, Zhu J, Kulich SM, Chu CT. Mitochondrially localized ERK2 regulates mitophagy and autophagic cell stress: implications for Parkinson's disease. Autophagy 2008; 4: 770-82.
[252] Choi SY, Kim JY, Kim HW, Cho B, Cho HM, Oppenheim RW, Kim H, Rhyu IJ, Sun W. Drp1-mediated mitochondrial dynamics and survival of developing chick motoneurons during the period of normal programmed cell death. FASEB J 2013; 27: 51-62.
[253] Yuan H, Gerencser AA, Liot G, Lipton SA, Ellisman M, Perkins GA, Bossy-Wetzel E. Mitochondrial fission is an upstream and required event for bax foci formation in response to nitric oxide in cortical neurons. Cell Death Differ 2007; 14: 462-71.
[254] Kitami T, Logan DJ, Negri J, Hasaka T, Tolliday NJ, Carpenter AE, Spiegelman BM, Mootha VK. A chemical screen probing the relationship between mitochondrial content and cell size. PloS one 2012; 7: e33755.
[255] Rossignol R, Gilkerson R, Aggeler R, Yamagata K, Remington SJ, Capaldi RA. Energy substrate modulates mitochondrial structure and oxidative capacity in cancer cells. Cancer Res 2004; 64: 985-93.
[256] Koopman WJ, Verkaart S, van Emst-de Vries SE, Grefte S, Smeitink JA, Willems PH. Simultaneous quantification of oxidative stress and cell spreading using 5-(and-6)-chloromethyl-2',7'-dichlorofluorescein. Cytometry A 2006; 69: 1184-92.
[257] Blanchet L, Buydens MC, Smeitink JA, Willems PH, Koopman WJ. Isolated mitochondrial complex I deficiency: explorative data analysis of patient cell parameters. Curr Pharm Des 2011; 17: 4023-33.
[258] Itoh K, Nakamura K, Iijima M, Sesaki H. Mitochondrial dynamics in neurodegeneration. Trends Cell Biol 2013; 23: 64-71.

[259] Rambold AS, Kostelecky B, Elia N, Lippincott-Schwartz J. Tubular network formation protects mitochondria from autophagosomal degradation during nutrient starvation. Proc Natl Acad Sci USA 2011; 108: 10190-5.
[260] Szabadkai G, Simoni AM, Chami M, Wieckowski MR, Youle RJ, Rizzuto R. Drp-1-dependent division of the mitochondrial network blocks intraorganellar Ca2+ waves and protects against Ca2+-mediated apoptosis. Mol Cell 2004; 16: 59-68.
[261] Song W, Bossy B, Martin OJ, Hicks A, Lubitz S, Knott AB, Bossy-Wetzel E. Assessing mitochondrial morphology and dynamics using fluorescence wide-field microscopy and 3D image processing. Methods 2008; 46: 295-303.
[262] Schuelke M, Smeitink J, Mariman E, Loeffen J, Plecko B, Trijbels F, Stockler-Ipsiroglu S, van den Heuvel L. Mutant NDUFV1 subunit of mitochondrial complex I causes leukodystrophy and myoclonic epilepsy. Nat Genet 1999; 21: 260-1.

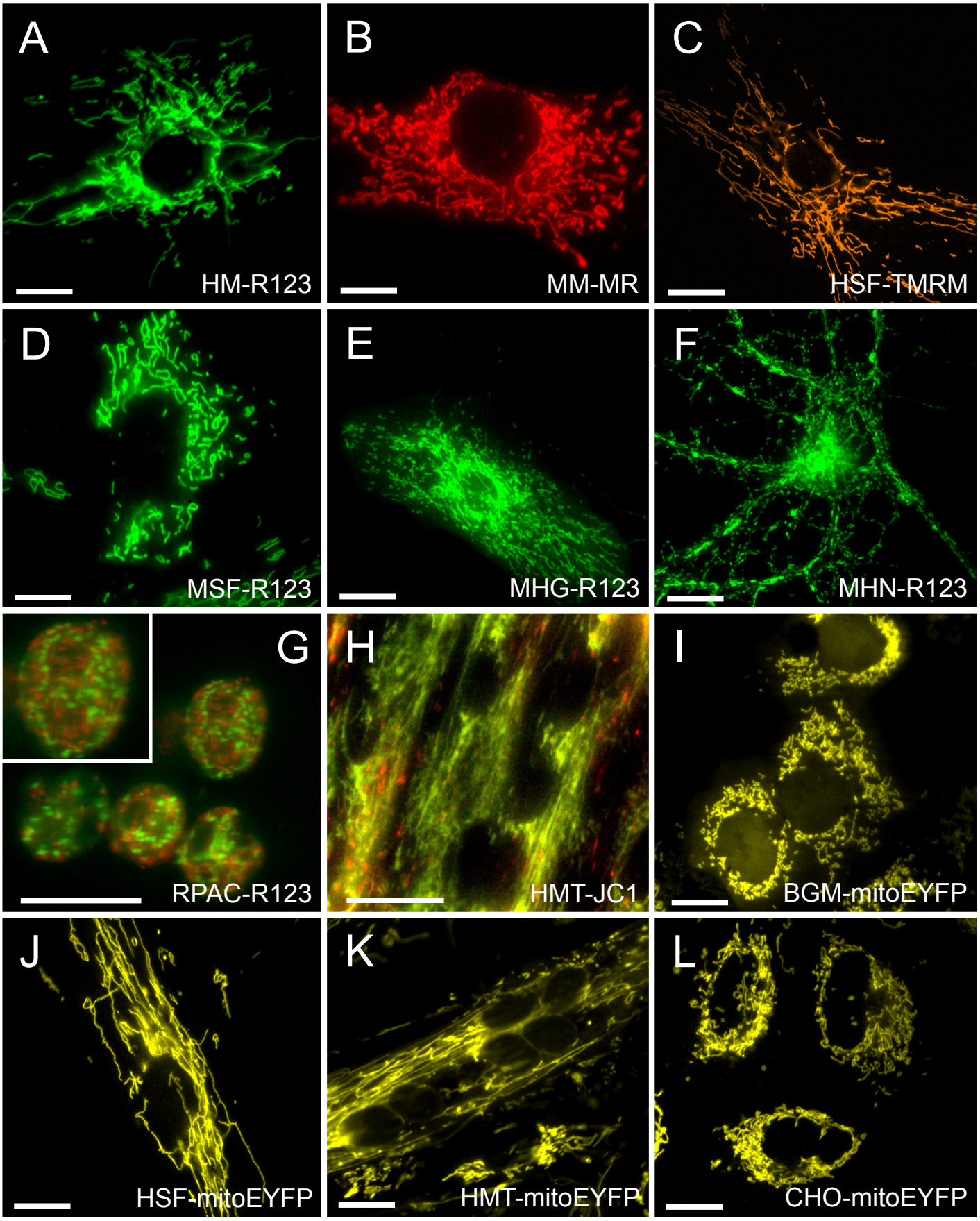

Tronstad et al,. Fig. 1

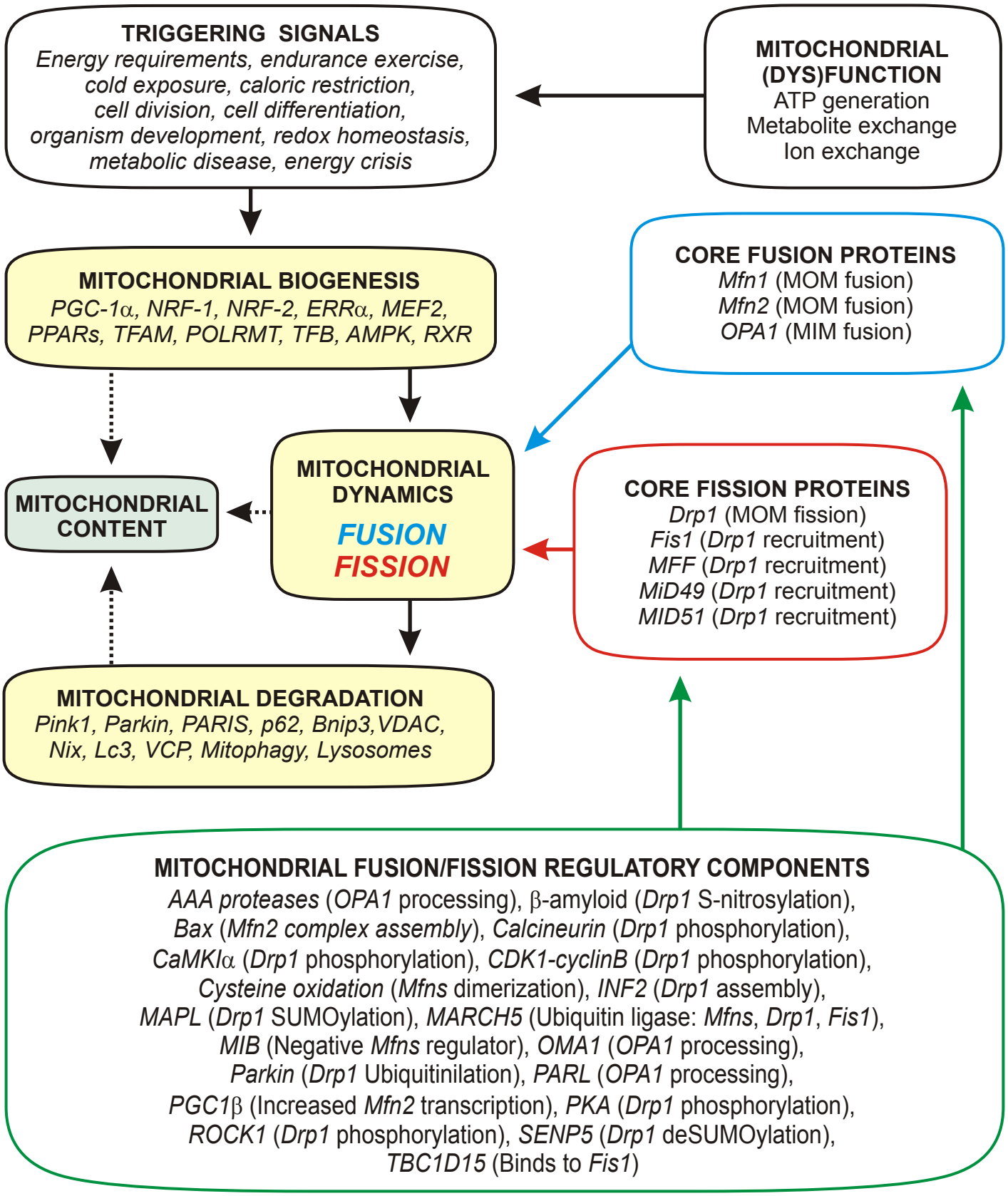

Tronstad et al,. Fig. 2

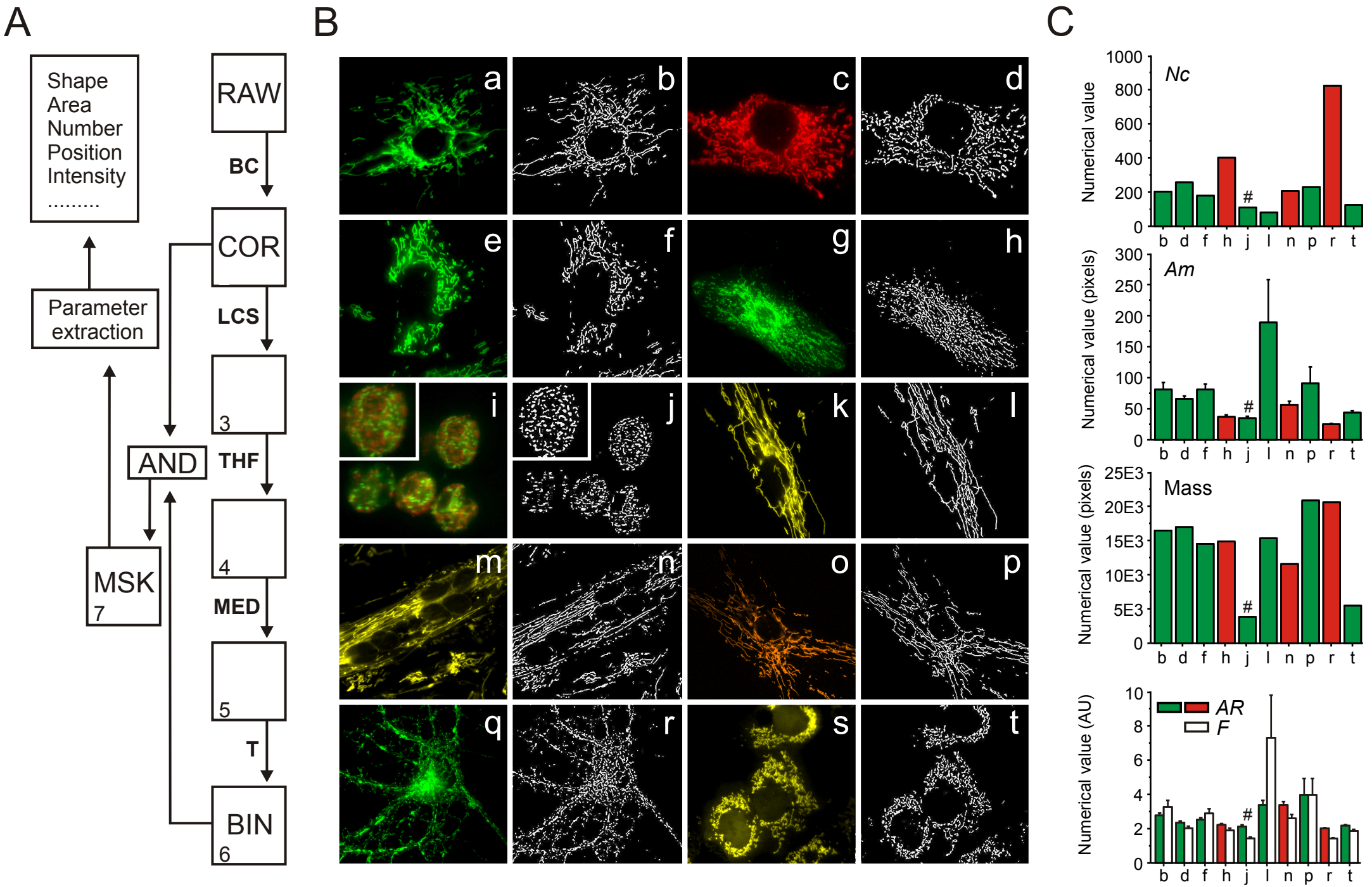

Tronstad et al,. Fig. 3

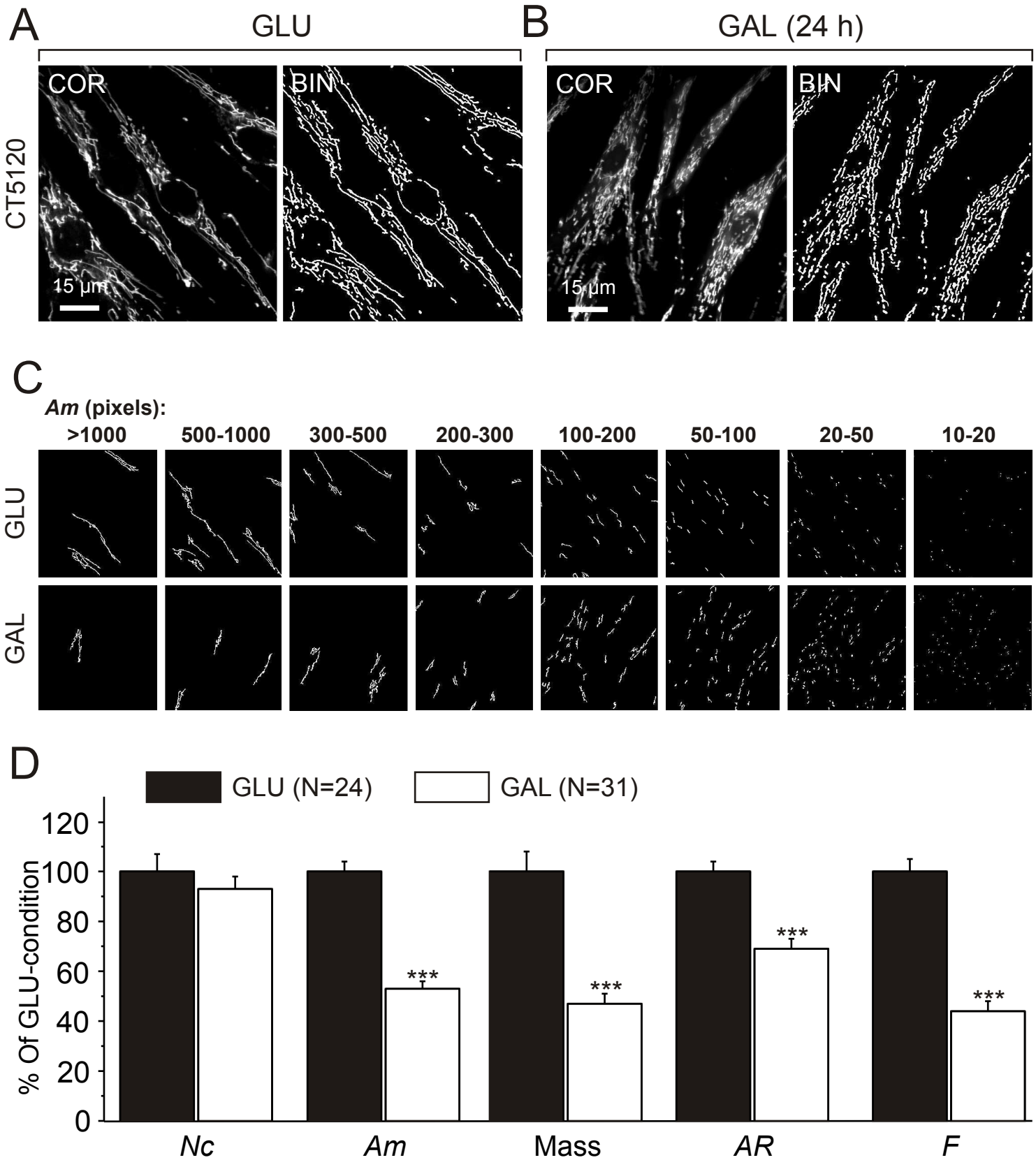

Tronstad et al,. Fig. 4

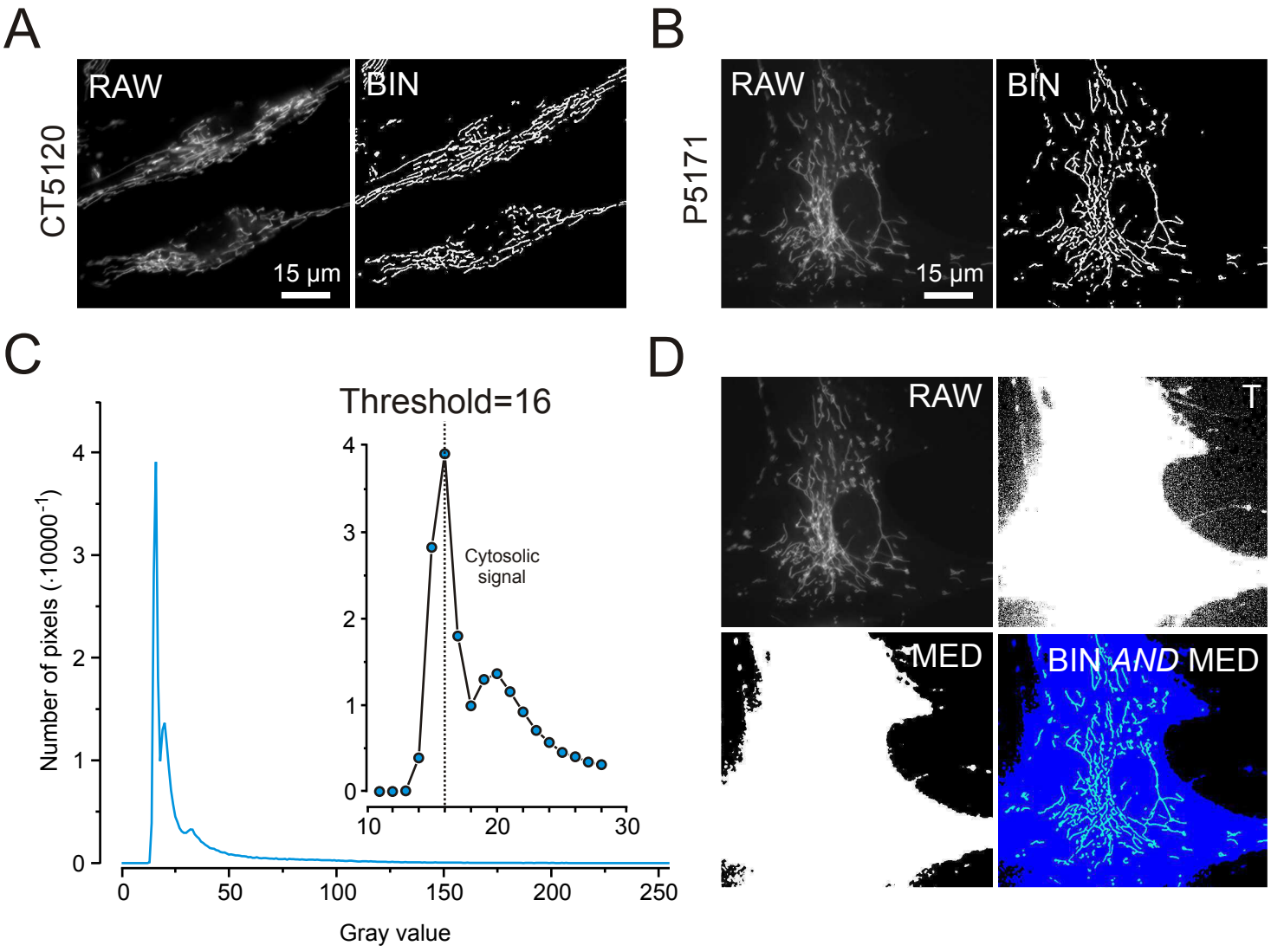

Tronstad et al,. Fig. 5

A

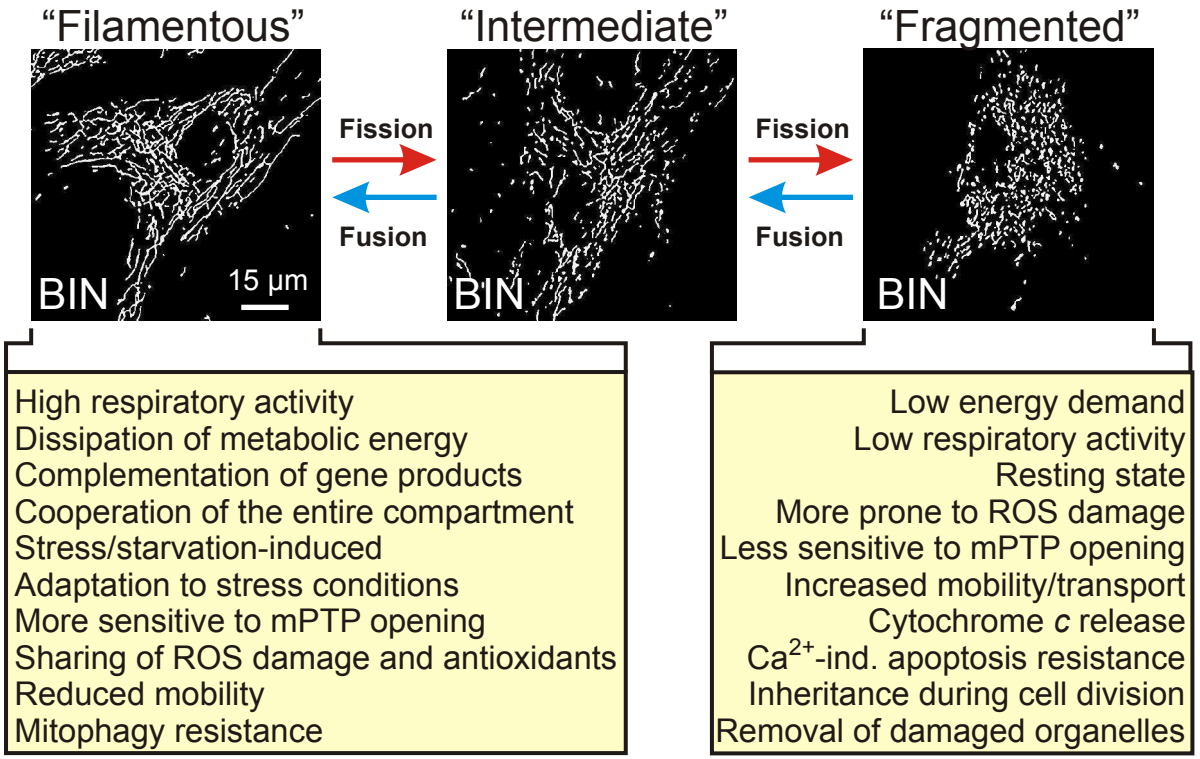

B

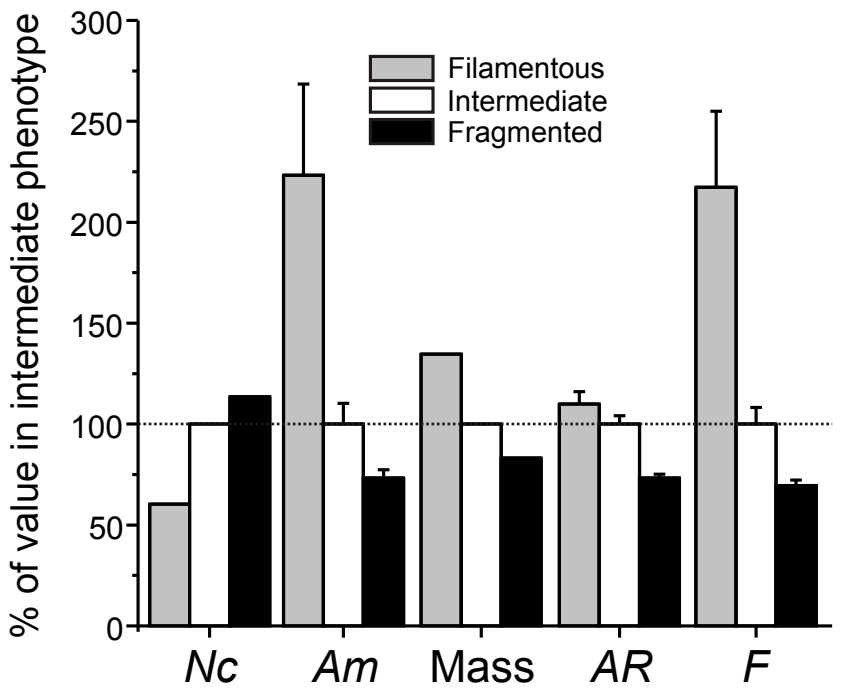

C

Morphology phenotype	*Nc*	*Am*	Mass	*AR*	*F*
Filamentous	Normal/reduced	Increased	Increased	Normal/Increased	Increased
Intermediate	Normal	Normal	Normal	Normal	Normal
Fragmented	Increased	Reduced	Normal/reduced	Reduced	Reduced
Elongation	Normal	Increased	Normal/increased	Increased	Increased
Shrinkage	Normal	Reduced	Normal/reduced	Reduced	Reduced
Biogenesis	Normal/increased	Normal/increased	Increased	Normal/increased	Normal/increased
Incr. fusion	Reduced	Increased	Normal/increased	Normal/increased	Normal increased
Incr. fission	Increased	Reduced	Normal/reduced	Normal/reduced	Normal/reduced

Tronstad et al,. Fig. 6

Table.1: Selected examples of pharmacological modulation of mitochondrial morphology and mass in mammalian cells

Species	Tissue/Cell type	Treatment/condition	Mechanism	Methods and measurements	Mitochondrial effects	Refs
Human	Cancer and non-cancer cell lines, HUVECs	AICAR	AMPK, AKT	Biochemical biomarkers, Microscopy	Increased content and functionality Cell-type dependent effects	[25, 32]
Human	HeLa 143B MDA-MB-231	Bezafibrate	Mitochondrial biogenesis, PPARs	Bioenergetic capacity, Biochemical biomarkers, Microscopy	Increased content and functionality	[26]
Human	CEM cells	d4T, ddC, ddI	Cell stress/death	mtDNA, microscopy	Reduced content, normal morphology	[27]
Human/ Rat/ Mouse	U937, L6, PC12 $eNOS^{-/-}$ mice	DETA-NO	Mitochondrial biogenesis, NO	Bioenergetic capacity, Biochemical biomarkers,	Increased content and functionality	[28]
Human	MRC-5	H_2O_2	ROS	mtDNA, flow cytometry	Increased content	[29]
Human	HUVECs	Homocysteine	ROS, NF-kappaB	Biochemical biomarkers, Microscopy	Increased content	[30]
Rat	Enriched cortical neurons /Primary neuronal cultures	LPS ,Transient oxygen & glucose deprivation	TFAM, AMPK, AKT	Bioenergetic capacity, Biochemical biomarkers, Microscopy	Increased content and functionality	[31]
Human	HUVECs	Metformin	Mitochondrial biogenesis, AMPK	Biochemical biomarkers, Microscopy	Increased content	[32]
Mice	Skeletal Muscle C2C12 cells	Rapamycin	mTOR, PGC1a	Bioenergetic capacity, Biochemical biomarkers	Reduced content and functionality	[33]
Mice	Skeletal muscle MEFs	Resveratrol	Mitochondrial biogenesis, autophagy, SIRT1, PGC-1α, NRF-1	Bioenergetic capacity, Biochemical biomarkers	Increased content and functionality	[34, 35]
Mouse	3T3-L1 cells	Rosiglitazone	Mitochondrial biogenesis, PPARs	Bioenergetic capacity, Biochemical biomarkers, Microscopy	Increased content and functionality	[36]
Human	Primary skin fibroblasts	Rotenone	ROS and lipid peroxidation increases?	Biochemical biomarkers, Microscopy	Increased length and degree of branching	[37]
Human	Primary skin fibroblasts	Trolox	Mfn2 level increase	Biochemical biomarkers, Microscopy	Increased length and degree of branching and functionality	[38]
Rat	Liver, hepatocytes	TTA	PPARs, mTOR	Bioenergetic capacity, Biochemical biomarkers, Microscopy	Increased content and functionality	[39-41]

Abbreviations: AICAR, 5-aminoimidazole-4-carboxamide riboside, AKT, v-akt murine thymoma viral oncogene homolog, AMPK, AMP-dependent protein kinase, d4T, 2',3'-didehydro-3'-deoxythymidine, ddC, 2',3'-dideoxycytidine, ddI, 2',3'-dideoxyinosine, DETA-NO, (Z)-1-[2-(2-aminoethyl) -N-(2-ammonioethyl) amino]diazen-1-ium-1,2 diolate, eNOS, endothelial nitric oxide synthase, HUVECs, human umbilical vein endothelial cells, LPS, lipopolysaccharide, MEFs, mouse embryonic fibroblasts, Mfn2, mitofusin 2, mtDNA, mitochondrial DNA, mTOR, mammalian target of rapamycin, NO, nitric oxide, NRF-1, nuclear respiratory factor-1, PGC-1α, peroxisome proliferator-activated receptor gamma coactivator-1α, PPARs, peroxisome proliferator-activated receptors, ROS, reactive oxygen species, SIRT1, silent mating type information regulation 2 homolog 1, TFAM, Transcription factor A, mitochondrial, Trolox, 6-hydroxy-2,5,7,8-tetramethylchroman-2-carboxylic acid, TTA, Tetradecylthioacetic acid.

Table 2: Selected studies applying quantitative analysis of mitochondrial morphology parameters

Cell type	Mode	Staining	Microscopy	Algo	Parameters	Refs
PHSF	2D	R123-pulse	Video-rate CLSM	A	*Am, AR, F, Nc, F/Nc, Mass, width, length*	[37, 149, 150, 162, 222, 225]
PHSF	2D	TMRM	Epifluorescence	A	*Am, AR, F, Nc, width, length*	[38, 219, 226-228]
PHSF	2D	MitoGFP	Epifluorescence	A	*Am, AR, F, Nc, width, length*	[219]
PHSF	2D	MitoEYFP	CLSM	A	*F, Nc, F/Nc*	[229]
PHSF	2D	Anti-GRP75	Epifluorescence	A	*F*	[230, 231]
N2a	2D	R123-pulse	Video-rate CLSM	A	*AR, F, Nc*	[232]
PHMyob	2D	R123-pulse	Video-rate CLSM	A	*AR, F, Nc*	[233]
HeLa	2D	R123-pulse	Video-rate CLSM	A	*F, Nc*	[38, 218]
SH-SY5Y	2D	MitoDsRed2	CLSM	A	*AR*	[234]
SH-SY5Y	2D	MitoDsRed2	CLSM	A	*AR*	[235]
PMEFs	2D	TMRM	Epifluorescence	A	*Am, F, Nc, Mass*	[236]
CHO	2D	TMRM	Epifluorescence	A	*F, Nc*	[38]
IMEFs	2D	TMRM	Epifluorescence	A	*F, Nc*	[38]
CEA	2D	TMRM	CLSM	A	*Am, AR, Nc*	[237]
CEH	2D	TMRM	CLSM	A	*Am, AR, Nc*	[237]
CEMC	2D	MitoGFP	CLSM	A	*AR, F*	[238]
M17HN	2D	MitoDsRed2	CLSM	A	*AR*	[239]
CV1	2D	MitoDsRed	Epifluorescence	B	*AR*	[240, 241]
C9, H9c2	2D	RFP	Epifluorescence	B	*AR, F*	[242]
H9c2	2D	Mitotracker Red	Epifluorescence	B	*AR, F*	[243]
C9, H9c2	2D	Various	Epifluorescence	B	*AR, F*	[244]
MM	2D	MitoroGFP2	Epifluorescence	B	*Am, F, P*	[245]
U2OS	2D	MitoDsRed2	CLSM	B	*Length, Am, Mass, others*	[246]
PHSF	3D	MitoDsRed2	Epifluorescence + decon.	C	*V, BP, Nc, NPC*	[247]
HUVEC	2D	Mitotracker Green	Epifluorescence	D	*AR, F, length*	[248]
CHO	2D	MitoDsRed	Epifluorescence	E	*Morphology, skeleton, and binary texture features*	[249]
PC12	2D	MitoDsRed2	Epifluorescence	F	*Am, Nc, length*	[250]
SH-SY5Y	2D	Mitotracker Red	CLSM	G	*TMA*	[251]
CEMN	2D	MitoDsRed	CLSM	H	*Am, Nc*	[252]
RCN	2D	MitoDsRed2	Epifluorescence	I	*Nc, length*	[253]

Quantification algorithms: A = [37, 162, 219, 222]; B = Variant of algorithm A; C = [247]; D = [248]; E = [249]; F = [250]; G = [251]; H = [252]; I = [253] **Abbreviations:** AFM, atomic force microscopy; Algo, mitochondrial morphology quantification algorithm; *Am,* mitochondrial area (size); *AR*, aspect ratio; *BP*, mitochondrial branching points; C9, clone 9 rat liver cell; CEA, chicken embryo astrocytes; CEH, chicken embryo hepatocytes; CEMC, *C. elegans* muscle cells; CEMN, chick embryo motor neurons; CHO, Chinese hamster ovary; CLSM, confocal laser scanning microscopy; CV1, monkey kidney fibroblast cells; decon, deconvolution; *F*, formfactor; *F/Nc*, mitochondrial complexity; GRP75, mitochondrial heatshock protein 70 (mtHSP70); H9c2, cardiac myoblast cell; HUVEC, human umbilical vein endothelial cell; IMEF, immortalized mouse embryonic fibroblast; IRHM, isolated rat heart mitochondria; MitoEYFP, mitochondria-targeted enhanced yellow fluorescent protein; MitoGFP, mitochondria-targeted green fluorescent protein; MitoroGFP2, mitochondria-targeted redox-sensitive green fluorescent protein 2; M17HN, M17 human neuroblastoma; MM, malignant mesothelioma; n.a., not appropriate; N2a, mouse neuroblastoma cell line; *Nc*, number of mitochondria per cell; *NPC,* mitochondrial networks per cell; *P*, mitochondrial perimeter; PC12, rat pheochromocytoma cell; PHMyob, primary human myoblasts; R123, rhodamine 123; RCN, rat cortical neurons; PHSF, primary human skin fibroblasts; PMEF, primary mouse embryonic fibroblast; RFP, red fluorescent protein; SH-SY5Y, human dopaminergic neuroblastoma clonal cell; TMA, total mitochondrial area; TMRM, tetramethylrhodamine methylester; U2OS, human osteosarcoma cell line; *V*, mitochondrial volume.